GEOLOGICA CARPATHICA, AUGUST 2020, 71, 4, 291–313 https://doi.org/10.31577/GeolCarp.71.4.1

The late Badenian–Sarmatian (Serravallian) environmental transition calibrated by sequence stratigraphy (eastern Danube Basin, Central Paratethys)

PETRONELA NOVÁKOVÁ[1, ✉], SAMUEL RYBÁR[1], KATARÍNA ŠARINOVÁ[2], ALEXANDER NAGY[3], NATÁLIA HUDÁČKOVÁ[1], MICHAL JAMRICH[1], VASILIS TEODORIDIS[4], MARIANNA KOVÁČOVÁ[1], MICHAL ŠUJAN[1], TOMÁŠ VLČEK[1] and MICHAL KOVÁČ[1]

[1]Department of Geology and Paleontology, Faculty of Natural Sciences of Comenius University, Mlynská dolina, Ilkovičova 6, Bratislava, Slovakia; ✉novakova148@uniba.sk
[2]Department of Mineralogy and Petrology, Comenius University in Bratislava, Mlynská dolina, Ilkovičova 6, 842 15 Bratislava, Slovakia
[3]Department of Younger Geological Formations, State Geological Institute of Dionýz Štúr, Mlynská dolina 1, Bratislava, Slovakia
[4]Department of Biology and Environmental Studies, Charles University, Magdalény Rettigové 4, 116 39 Prague, Czech Republic

(Manuscript received February 19, 2019; accepted in revised form June 18, 2020; Associate Editor: Adam Tomašových)

Abstract: The late Badenian and Sarmatian (Serravallian) evolution of depositional environments in the Danube Basin (Želiezovce Depression) has never been fully explored. Here, we clarify the paleoenvironmental changes which took place in this area during the late Badenian and Sarmatian on the basis of sedimentological, petrographic, biostratigraphic and paleobotanical analyses performed at multiple sections. The combination of these methods with sequence stratigraphy allowed us to divide the sedimentary record into three main intervals: 1) the transgressive late Badenian rocky shore deposits (transgressive and/or highstand system tract), followed by a gap in the stratigraphic record (that can approximately coincide with the latest Badenian falling stage system tract). 2) Earliest Sarmatian terrestrial deposits connected with the beginning of the Sarmatian transgression (synchronous with the lowstand system tract). 3) The early Sarmatian deltaic environment influenced by tidal processes associated with the highstand system tract. The fossil leaf association indicates a climatic turnover from subtropical to temperate conditions between the earliest (lowstand system tract) and the early Sarmatian (highstand system tract). Sediments of the late Sarmatian (falling stage system tract) were not deposited or were later eroded. However, they may be present in the neighbouring depressions, which tectonically opened during the late Sarmatian. The Badenian–Sarmatian boundary in the Želiezovce Depression is developed in transgressive shallow marine to terrestrial volcano-sediments as is typical for this boundary in most other Paratethys depocentres.

Keywords: Serravallian, Danube Basin, Želiezovce depression, sequence stratigraphy, sedimentology, biostratigraphy, paleobotany.

Introduction

The north-western part of the Pannonian Basin System is represented by the Danube Basin bordered by the Eastern Alps, Western Carpathians and Transdanubian Central Range. The northern part of the Danube Basin is divided into four partial depressions (Vass 2002; Fig. 1), which were opened in several tectonic events during the Miocene (Hók et al. 2016). The presented study will focus on the Želiezovce Depression that was formed during the early Badenian (Langhian; ~15.1 Ma; Sant et al. 2017, 2020; Rybár et al. 2019; Figs. 1, 2) and was filled up during the middle and late Miocene (Kováč et al. 2018). The neighbouring Komjatice Depression was opened during a younger tectonic phase (~12 Ma; Hók et al. 2016; Šarinová et al. 2018), where the Mojmírovce fault system created new accommodation space filled up by shelf-break slope and stable submarine platform sediments (Šarinová et al. 2018).

A major sea level drop, dated to 12.6 Ma, is linked with the Badenian–Sarmatian (intra Serravallian) extinction event (BSEE), which occurred in the Central Paratethys Sea (Harzhauser & Piller 2007; Holcová 2008; Paulissen et al. 2011; Mandic et al. 2018). In the scope of the Danube Basin, this sea level fall is documented by a transition from marine to brackish settings (e.g., Kováč 2000; Rybár et al. 2016). However, this sea level fall is not fully documented in the Želiezovce Depression. The *Ervillia* Zone typical of the Sarmatian was documented in Kováč et al. (2018) but sediments of this zone were not connected with surface exposures. Therefore, the main aim is to reveal the environmental changes that took place during the late Badenian and Sarmatian in the Želiezovce Depression on the basis of sedimentological, petrographic, biostratigraphic and paleobotanical analyses and using the 3rd order sequence stratigraphic framework calibrated for the Central Paratethys by Hohenegger et al. (2014; Fig. 2).

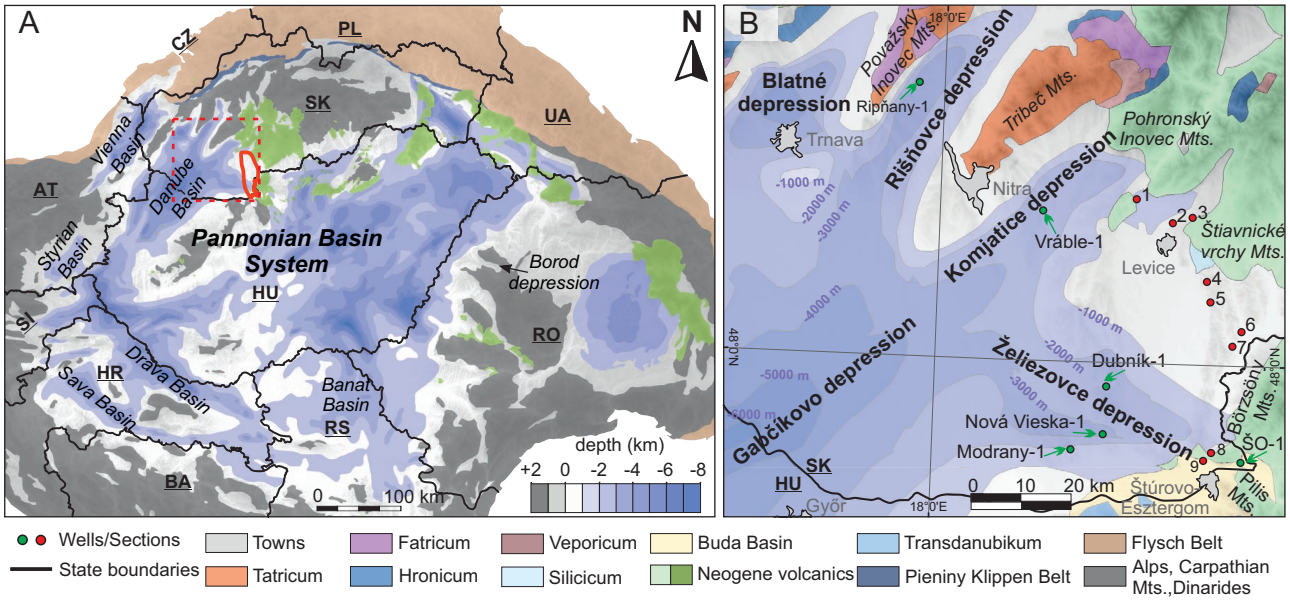

Fig. 1. Location maps of the studied area. **A** — Location of the study area in the Alpine–Carpathian–Pannonian system. **B** — Location of wells and sections in the eastern Danube Basin (for explanations of the section names see Fig. 2; modified after Fusán et al. 1987; Hók et al. 2014; Horváth et al. 2015).

Geological setting

The Miocene sedimentation in the eastern part of the Danube Basin (Fig. 2) starts with the earliest Badenian (the earliest Langhian) Bajtava and Špačince formations, which discordantly overlie the pre-Neogene basement composed of Paleozoic crystalline rocks of the Veporic unit and the Paleogene sediments of the Hungarian Paleogene Basin (Tari et al. 1993). The Bajtava and Špačince formations are difficult to distinguish from each other in this part of the basin. They are both formed by marine deposits and volcaniclastics from the Börzsöny, Štiavnica and Krupina volcanic fields (Vass 2002; Kováč et al. 2018). These deposits are overlain by the Pozba and Vráble formations (upper Badenian–Sarmatian, Serravallian) that were deposited in a marine shelf environment with transition to deltaic sediments (Vass 2002; Kováč et al. 2018). Subsequently, Pannonian (Tortonian) sediments accumulated in brackish to lacustrine, deltaic and alluvial environments (Ivanka Fm., Beladice Fm., Volkovce Fm.; Šujan et al. 2016; Sztanó et al. 2016). The deposition in this area terminates with the Pliocene to Pleistocene sediments of the Kolárovo Formation (Šujan et al. 2016; Sztanó et al. 2016).

Methods

The sections were levelled by palette-knife and cleaned by sash brushes. Photo documentation of each layer was done by SLR Camera. The sedimentary layers were then subjected to facies analysis, with special attention given to fluid flow and soft-sediment deformation. These observations were then used for interpretation of transport mechanisms and for determination of paleoenvironmental conditions (Boggs 2006; Nichols 2009; Rossi et al. 2017). Cross-stratification dip data were measured and displayed in standard rose diagrams (Collinson & Thompson 1989). Facies codes were adopted mainly from Miall (2006) and extended based on Rossi et al. (2017) and Németh & Martin (2007), where the capital letter indicate dominant grain size and the lowercase letters characterize texture or structure of the lithofacies (Fig. 3). Granulometric analysis was done using particle sizer analyser Mastersizer 3000 (Sedimentological laboratory, Department of Sedimentology and Paleoenvironmental analysis; Jagiellonian University, Kraków).

For petrography, the selected samples were studied under a polarizing microscope. The tuff samples were studied by microprobe CAMECA SX 100 (State Geological Institute of Dionýz Štúr). The heavy fraction was separated using heavy liquid from the 0.25–0.10 mm fraction (10 g) and studied under the binocular microscope. The terminology used in the subdivision of 3rd order sequences to system tracts follows Coe (2003, i.e., the sequence boundary is located between the HST and FSST).The geochronological assignments of system tract boundaries follow Hohenegger et al. (2014), who relied on Hardenbol et al. (1998).

Calcareous nannofossils were studied from smear slides prepared by a standard quantitative method (Bown 1998). A portion of sediment was mixed with distilled water on a glass slide with a toothpick to create a thick suspension. The suspension was smeared thinly across the coverslip with the toothpick and dried on a hotplate. Later coverslip was affixed using Norland 61optical adhesive and glued under UV light. The samples were analysed using Olympus BX50 microscope at 1250× magnification. A camera Olympus Infinity 2 with QuickPHOTO CAMERA 2.3 software was used for the photographic record. Specimens were counted

at 300 fields of view (FOV) using a quantitative method. Systematic identification of calcareous nannofossils was done using the taxonomy of Young (1998) and Young et al. (2017). Standard nannofossil NN zonation (Martini 1971) was used for age determination.

Foraminifers were obtained from 200 g of material treated with H_2O_2 (10 %) and subsequently sieved with a mesh size of 1.25 and 0.071 mm. A combination of the binocular stereoscopic microscope (Olympus SZ75), the biological polarizing microscope and the scanning electron microscope QUANTA FEG 250 were used during determination and imaging (e.g., Kováčová & Hudáčková 2009). The taxonomical approach followed Loeblich & Tappan (1992), Cicha et al. (1998) and Holbourn et al. (2013). The paleoecological parameters of the obtained foraminiferal assemblages were evaluated on the basis of the presence and dominance of taxa exhibiting special environmental significance (Boltovskoy & Wright 1976; Murray 2006).

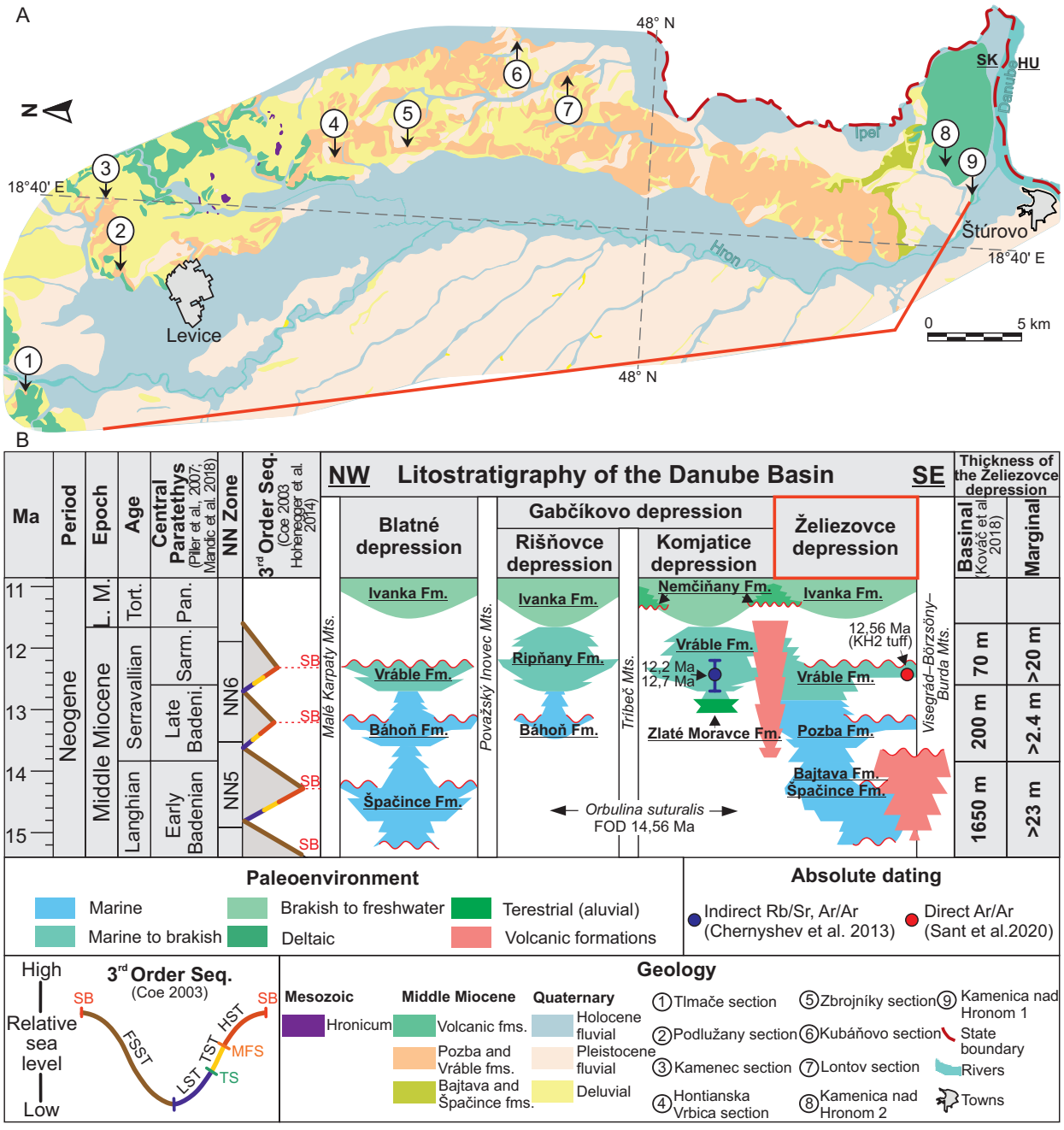

Fig. 2. A — Geological map of the study area with position of the sections (modified after Káčer et al. 2005). **B** — Lithostratigraphic scheme (palaoenvironment is modified after Fordinál & Elečko 2000; Vass 2002; Rybár et al. 2016; Šarinová et al. 2018; Kováč et al. 2018; geology is modified after Káčer et al. 2005; marginal thickness of the basin is extracted from this study; the terminology of 3rd order sequences follows Coe 2003; timing of the regression–transgression events was adopted from Hohenegger et al. 2014, who relied on Hardenbol et al. 1998).

Lithofacies code	Lithofacies	Sedimentary textures	Depositional process, interpretation
Gmm	Gravel, matrix supported	Massive	Debris flow, lahar
Gmg	Gravel, matrix supported	Indistinct gradation	Plastic debris flow
Gcm	Gravel, clast supported	Massive	Wave reworking, rocky shore
Gcg	Gravel, clast supported	Gradation	Alluvial fan, fan delta, traction transport
Gg	Gravel, clast supported	Indistinct gradation	Debris flow, alluvial fan
Gt	Gravel, stratified	Trough cross-stratification	Channel fills, traction transport
Gp	Gravel, fine to coarse, stratified	Planar cross-stratification	Tide dominated transverse bedforms, deltaic, traction tr.
Sm	Sand, very fine to coarse	Massive, faint lamination, bioturbation	Shallow marine, tide dominated
Sl	Sand, very fine to coarse	Rhythmic lamination	Tide dominated coast
St	Sand, fine to very coarse, may be pebbly	Trough cross-stratification	Sinuous-crested and linguoid dunes (3D), traction transport
Sp	Sand, fine to very coarse, may be pebbly	Planar cross-stratification	Transverse dunes (2D), traction transport
Sr	Sand, very fine to coarse	Ripple-cross stratification	Ripples (lower flow regime), traction to suspension transport
Sla	Sand, very fine to coarse	Faint low-angle lamination	Scour fills, supercritical flow deposits
Fm	Silt, clay	Massive	Ephemeral lake with rare marine ingressions, suspension
F	Silt, clay	Massive	Alluvial plain, suspension
Fl	Silt, clay	Rhythmic lamination, rare bioturbation	Tide dominated coast, suspension
Ct	Coarse tuff	Massive	Pyroclastic deposits
Lt	Lapilli tuff	Massive	Pyroclastic deposits
Tb	Tuff breccia	Massive	Pyroclastic deposits

Fig. 3. Lithofacies codes (modified after Miall 2006; Németh & Martin 2007; Rossi et al. 2017).

Leaves were described using the current morphological terminology published by Ellis et al. (2009). Molluscs were determined according to Papp (1954), Strausz (1966), Švagrovsky (1971), Bałuk (1975, 1995, 1997, 2006), Schultz (2001, 2003, 2005), Harzhauser (2002), Mandic (2004) and Mikuž (2009). It needs to be noted, that the late Badenian taxa (e.g., *Ancilla glandiformis, Cerithium vulgatum, Linga columbella*) extend beyond the Badenian on the global scale. However, it is likely that they terminate at the Badenian–Sarmatian boundary (BSEE) in the Central Paratethys (Harzhauser & Piller 2007; Holcová 2008; Paulissen et al. 2011; Mandic et al. 2018).

Results

Fossil content

From the **Kamenica nad Hronom 1** section (KH1; Figs. 2, 4, 5A–D) the first samples were taken from lowermost lapilli tuff layer and tuff breccia (Fig. 4; samples KH1-1, KH1-2), which contain large fragments of sponge spicules (Fig. 6B), rare *Ammonia inflata*, molds of miliolid shells and fragments of chambers. The third sample was taken from the coarse tuff dated by $^{40}Ar/^{39}Ar$ (Fig. 4; sample KH1-3). The tuff includes fragments of foraminiferal tests, while the top of the layer yields a diverse plant assemblage (Fig. 7). This assemblage consists of morphologically variable leaves of *Daphnogene polymorpha*, two different leaf morphotypes of the *Laurophyllum* sp. 1 (slender and oblong leaves) and *Laurophyllum* sp. 2 (broadly ovate to obovate leaves) from the Lauraceae family. These leaves are associated with a finely serrated incomplete leaf corresponding to a morphotype of *Ternstroemites* sp., which has a taxonomical affinity to Theaceae family. Echinoid spines and bryozoans also occur in the fossil assemblage (Fig. 4; sample KH1-3). Two samples were taken from the **Kamenica nad Hronom 2** section (KH2; Figs. 2, 4, 5E; samples KH2-1, KH2-2). Epiphytes prevail in foraminiferal assemblage, consisting of *Ammonia inflata*, *A. viennensis, Ammonia* sp., *Amphistegina* sp., *Asterigerinata planorbis, Hanzawaia boueana, Cibicidoides pachyderma, Elphidium crispum, Elphidium macellum*, *Glandulina ovula,*

Heterolepa dutemplei, Cycloforina badenensis, and *Miliolidae* sp. (Fig. 8F–H) Molluscs were collected from the entire height of the section from Gcm and Sm. The mollusc assemblage includes *Ancilla glandiformis, Cerithium vulgatum, Linga columbella*, and *Turritella* sp. (for more data on molluscs see chapter Biostratigraphy). Within the sandstone layer (Fig. 4; sample KH2-1), calcareous nannoplankton *Coccolithus pelagicus, Discoaster* cf. *exilis, Reticulofenestra minuta, Reticulofenestra haqii* and *Braarudosphaera bigelowii parvula* are observed. At the **Lontov** section, two samples were taken (Figs. 2, 4, 5F–H). The foraminiferal assemblage consists of *Elphidium reginum, E. josephinum, E. macellum*, *Schackoinella imperatoria*, *Ammonia parkinsoniana, A. viennensis, Bolivina antiqua, B. dilatata, Ciperoella ciperoensis, Globorotalia transsylvanica, Porosononion martkobi, Miliolidae* indet, and *Nonion* sp. (Fig. 8). Planktic species are abundant and are dominated by very small unidentified globigerinids. Foraminiferal shells are commonly recrystallized and rounded (Fig. 4; samples LON-1, LON-2). *Cerithium rubiginosum*, *Granulolabium bicinctum*, *Duplicata duplicate*, *Euspira helicina sarmatica,* and *Vitta picta* dominate in mollusc assemblages (Fig. 4; sample LON-2). Calcareous nannofossils are represented by *Braarudosphaera bigelowii parvula*, *Calcidiscus leptoporus*, *Calcidiscus pataecus*, *Coccolithus miopelagicus*, *Helicosphaera walbersdorfensis*, *Helicosphaera wallichii, Holodiscolithus macroporus, Reticulofenestra pseudoumbilicus* >8 μm, *Rhabdosphaera sicca, Sphenolithus heteromorphus,* and *Helicosphaera ampliaperta* (Fig. 4; samples LON-1, LON-2). Both samples additionally include ostracod shells, sponge spicules, diatoms, and radiolarians. Mollusc assemblage rich in individuals is present at the **Tlmače** section (Figs. 2, 4, 9A–C): *Mohrensternia* sp., *Rissoa* sp., *Abra* sp., *Inaeqnicostata politioanei suessiforme*, *Limnocardium* sp., *Loripes* sp., and *Loripes* aff. *dujardini* (Fig. 4; sample TL-2). The **Hontianska Vrbica** section (Figs. 2, 4, 9D–H; sample HON-2) contains a mollusc assemblage: *Cerastoderma* cf. *latisulcum*, *Cerastoderma latisulcum nexingense,* and *Cardiidae* indet. Sponge spicules and leaves are also present. Fossil assemblages at the **Kubáňovo** section (Figs. 2, 4, 10A–E; sample KUB-1) consist of both well preserved and strongly recrystallized foraminifera (*Ammonia inflata*, *Protoglobobulimina pupoides*, *Cancris auricula*, *Elphidium* sp., *Globigerina concinna*,

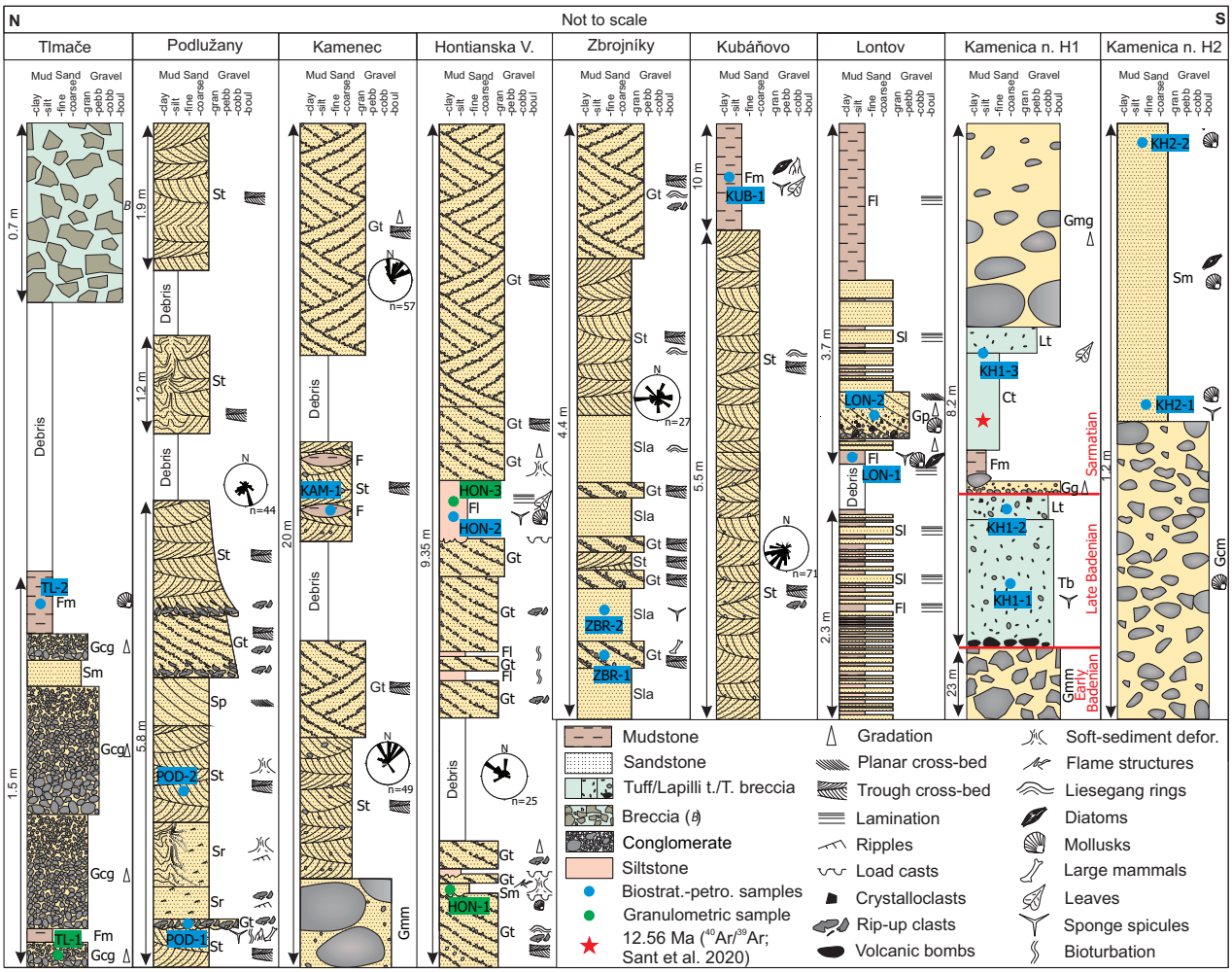

Fig. 4. Studied sections with paleoflow orientation marked in rose diagrams (the dated tuff is marked by a red star; sample name is KH2, Sant et al. 2020). For lithofacies codes and interpretations see Fig. 3.

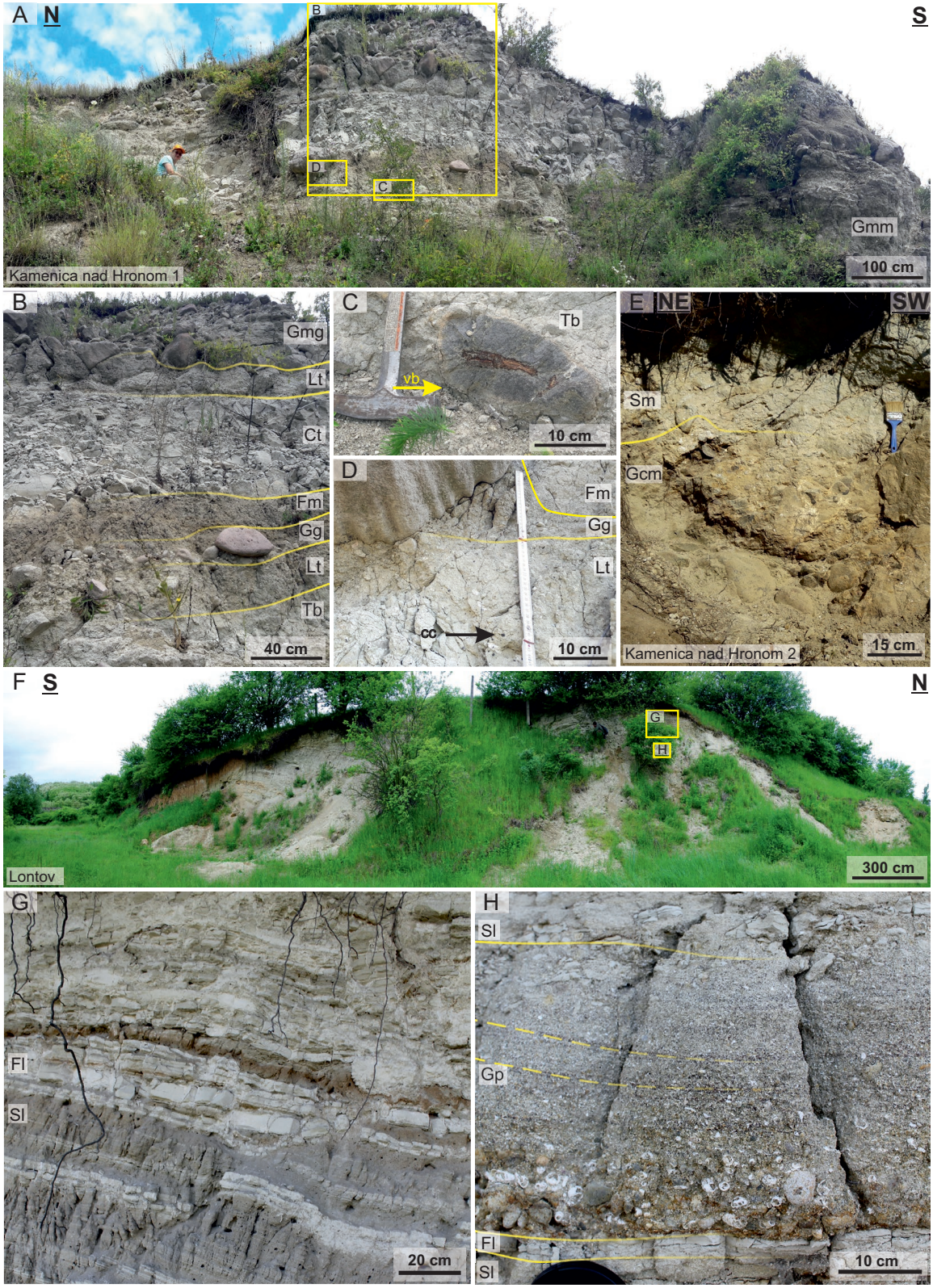

Fig. 5. Photoplate of the Kamenica nad Hronom 1, Kamenica nad Hronom 2 and Lontov sections. **A** — Overall view of the upper part of the Kamenica nad Hronom 1 section above the 23 cm-thick conglomerates. **B** — Lithofacies details of upper part of the section (between 8.2 and 0 m from the top). **C** — Arrow shows volcanic bomb (vb) present at the base of tuff breccia (8.2 m from the top). **D** — Arrow shows amphibole crystalloclasts (cc) in the lower lapilli tuff (between 8 and 7.2 m from the top). **E** — Kamenica nad Hronom 2 section with clast supported massive conglomerates and overlying massive sandstones (full section). **F** — Overall view of the Lontov section with marked position of lithofacies details. **G** — Alternation of rhythmic laminated sandstones and siltstones (between 2.7 and 0.7 m from the top). **H** — Detail of planar cross-bedded conglomerates with mollusc shells at the base (between 4.1 and 3.4 m from the top). For lithofacies codes and interpretations see Fig. 3.

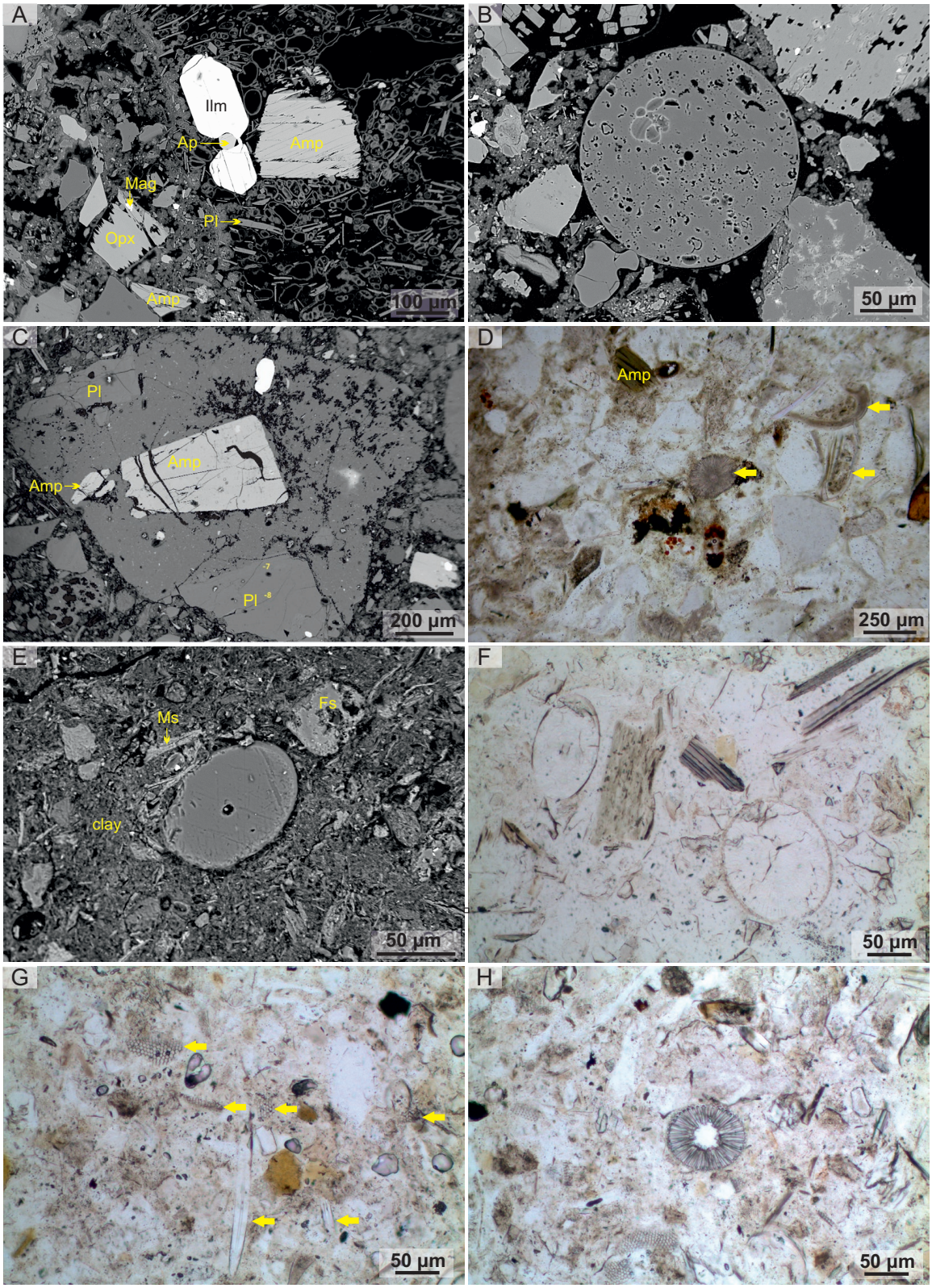

Fig. 6. Thin sections. **A** — Vesiculated volcanic lithoclasts in lower lapilli tuff from Kamenica nad Hronom 1 section (BSE). **B** — Sponge spicule in lower lapilli tuff from Kamenica nad Hronom 1 section (BSE). **C** — Volcanic lithoclast with amphibole and plagioclase phenocrysts in dated coarse tuff from Kamenica nad Hronom 1 section (BSE). **D** — Volcanic sandstones; yellow arrow shows diatoms and red arrow display calcareous nannofossils from Kamenica nad Hronom 2 section (PPL). **E** — Sponge spicule in siliceous mudstone from the Hontianska Vrbica section (BSE). **F** — Biogenic silica with sponge (left) and diatoms (right) in rhythmic laminated siltstone from Lontov section (PPL). **G, H** — Siliceous mudstone with sponge spicules and diatoms from Kubáňovo section (PPL). (PPL - plane polarized light, BSE - backscattered electron)

Globigerinoides sp.), abundant sponge spicules and diatoms, and less frequent radiolarians and leaves. Fossil assemblages at the **Kamenec** section (Figs. 2, 4, 10F–I) contain one agglutinated foraminifer taxon only (?*Ammobaculites* sp.?) and bivalve fragments (Fig. 4; sample KAM-1). **Zbrojníky** section (Figs. 2, 4, 11A–D) is very poor in fossil content, but the sample ZBR-2 (Fig. 4) includes a small amount of sponge spicules and the sample ZBR-1 (Fig. 4) contains a large mammal rib fragment. The sample from the **Podlužany** section (Figs. 2, 4, 11E–J; sample POD-1) contain sponge spicules and silicified remains of wood. This section is poor in foraminifera (*Fursenkoina* sp.) and clasts from intraformational conglomerate contain rhizoliths and large mammal bone fragments. The sample POD-2 was barren (Fig. 4; Suppl. Table S1).

Lithology

The lowermost part of the **KH1** section (Figs. 2, 4, 5A) consists of a ~23 m-thick poorly sorted volcaniclastic conglomerate (Gmm). Clasts reach boulder size (up to ~2 m in diameter) and the matrix is composed of sand. A 2 m-thick bed composed of tuff breccia follows (Tb; Fig. 5B,C), volcanic cobbles reach up to ~10 cm in diameter. Volcanic bombs occur (~40 cm in diameter) at the base of this tuff breccia. Higher up, a 40 cm-thick lapilli tuff (up to ~5 cm) with visible amphibole crystalloclasts occurs and its upper boundary is erosional. (Lt, Fig. 5B,D). The base of the next parasequence is composed of clast-supported gravels with indistinct normal gradation (Gg, Fig. 5B,D). The clasts size decreases from ~10–20 cm to ~3 cm in diameter. Additionally, rare boulders (~80 cm in diameter) are present at the upper boundary (Fig. 5B,D).

A ~45 cm-thick mud layer (Fm) overlies these coarsening upward gravels, followed by 150 cm-thick bed of massive tuff (Ct) dated by the $^{40}Ar/^{39}Ar$ method (Sant et al. 2020). The overlying lapilli tuff (Lt) is about ~40 cm thick and yields abundant fossil leaves at the base. The section continues with 3.2 m-thick, normally graded bed composed of matrix-supported clasts (Gmg, Fig. 5B). The rounded clasts are ~10–20 cm (occasionally ~40 cm) in diameter at the base and their size decreases upwards to ~5 cm. The matrix between the clasts is tuffaceous. The lower lapilli tuff (Fig. 4; sample KH1-2) is composed of volcanic lithoclasts, pumice fragments and crystalloclasts of plagioclase, amphibole, biotite and pyroxene. Chloritized tuffs and silts/wacke are rare. The volcanic lithoclasts with vitrophyric texture are composed of amphibole and plagioclase phenocrysts, which are accompanied by less frequent pyroxene, biotite, ilmenite and apatite (Fig. 6A). Some amphibole phenocrysts are rounded, possibly due to magmatic corrosion. Amphiboles are slightly zonal and magnesiohastinsite in composition (Fig. 12A; Suppl. Table S2). Both orthopyroxene (enstatite) and clinopyroxenes (pigeonite) are present (Fig. 12B; Suppl. Table S2). Plagioclase phenocrysts contain 77–89 % anorthite molecule (An; Fig. 12C; Suppl. Table S2). At high resolution, the glassy groundmass contains large amounts of vesicules and some plagioclase microliths ($An_{60–75}$). All vesicule margins (pumice and volcanic lithoclasts) show alteration.

The coarse tuff (Fig. 4; dated sample KH1-3) consists of angular to subangular grains composed of crystalloclasts of plagioclase, brown-green amphibole, biotite, pumice, and volcanic lithoclasts in a tuffaceous matrix. The volcanic lithoclasts with porphyric texture are composed of microlithic groundmass with plagioclase, biotite and amphibole phenocrysts (Fig. 6C). Pseudomorphs of pyroxene shape are rare. Based on their chemical compositions, amphiboles can be divided to two groups: hastingisite–sadanagaite and hornblende–tchermakite (Fig. 12A; Suppl. Table S2). Hornblende is considered juvenile. Volcanic lithoclasts with hastingsite phenocrysts and crystalloclast of sadanagaite were probably sourced from older volcanic rocks and from underlying lapilli tuff. Plagioclases are zonal, where central parts contain $An_{82–85}$ and marginal parts contain only $An_{50–67}$ (Fig. 12C; Suppl. Table S2). Nonvolcanic admixture is represented by polycrystalline quartz, biotite paragneiss, granitoid and shale.

The lower unit of the **KH2** section (Figs. 2, 4, 5E) is ~60 cm thick, and the lower boundary is unclear. It is composed of fossiliferous clast-supported conglomerate with rounded clasts up to pebble size (~2–20 cm in diameter; Gcm). Indistinct gradation is visible, and these conglomerates gradually pass into a 60 cm-thick, coarse-grained, bioturbated, massive sandstone (Sm) with faint lamination, which is terminated by a recent soil. The composition of clasts in both units is similar but the amount of andesite clasts decreases towards the top and the amount of quartz and calcareous fossils increases upwards. Andesite clasts are vitrophyric to porphyric, composed of phenocryst amphibole, plagioclase, biotite in vesiculated or microlithic groundmass (Fig. 6D). Andesite clasts, pumice and vitroclasts show various degrees of alternation. Sandy grains are formed by quartz, plagioclase, biotite, amphibole, muscovite, glauconite, rare pyroxene and zircon. High portion of calcareous and siliceous bioclasts is typical (Fig. 6D).

The lower part of the **Lontov** section (Figs. 2, 4, 5F) is 2.3 m thick and consists of rhythmic laminated siltstones (Fl) and sandstones (Sl; Fig. 5G). Both lithofacies are fossiliferous and the laminae occasionally vertically pass into beds, which are up to 15 cm thick. In the upper part of the section (3.7 m), similar lithofacies (Fl, Sl) continue with the exception of a planar, cross-stratified, 50 cm-thick bed (Gp), which is located 3.4 m from the top of the section (Fig. 5H). This fossiliferous bed is composed of conglomerates with pebble size clasts (~6 cm in diameter), that gradually pass into sands. The pebble size clasts are often formed by mollusc shells. In the uppermost 1.7 m of the section, the amount of sandstones (Sl) decreases and siltstones (Fl) dominate.

The siltstones (Fig. 4; sample LON-1) are composed of subangular to rounded silty to fine sandy grains in clay matrix. Quartz and altered grains of volcanic origin dominate. Biotite, chlorite, feldspar, and glauconite are also present. Calcareous (foraminifera, molluscs) and siliceous (diatoms, sponge spicules) fossil remnants are abundant (Fig. 6F). Dispersed carbonate cement is also present in the matrix.

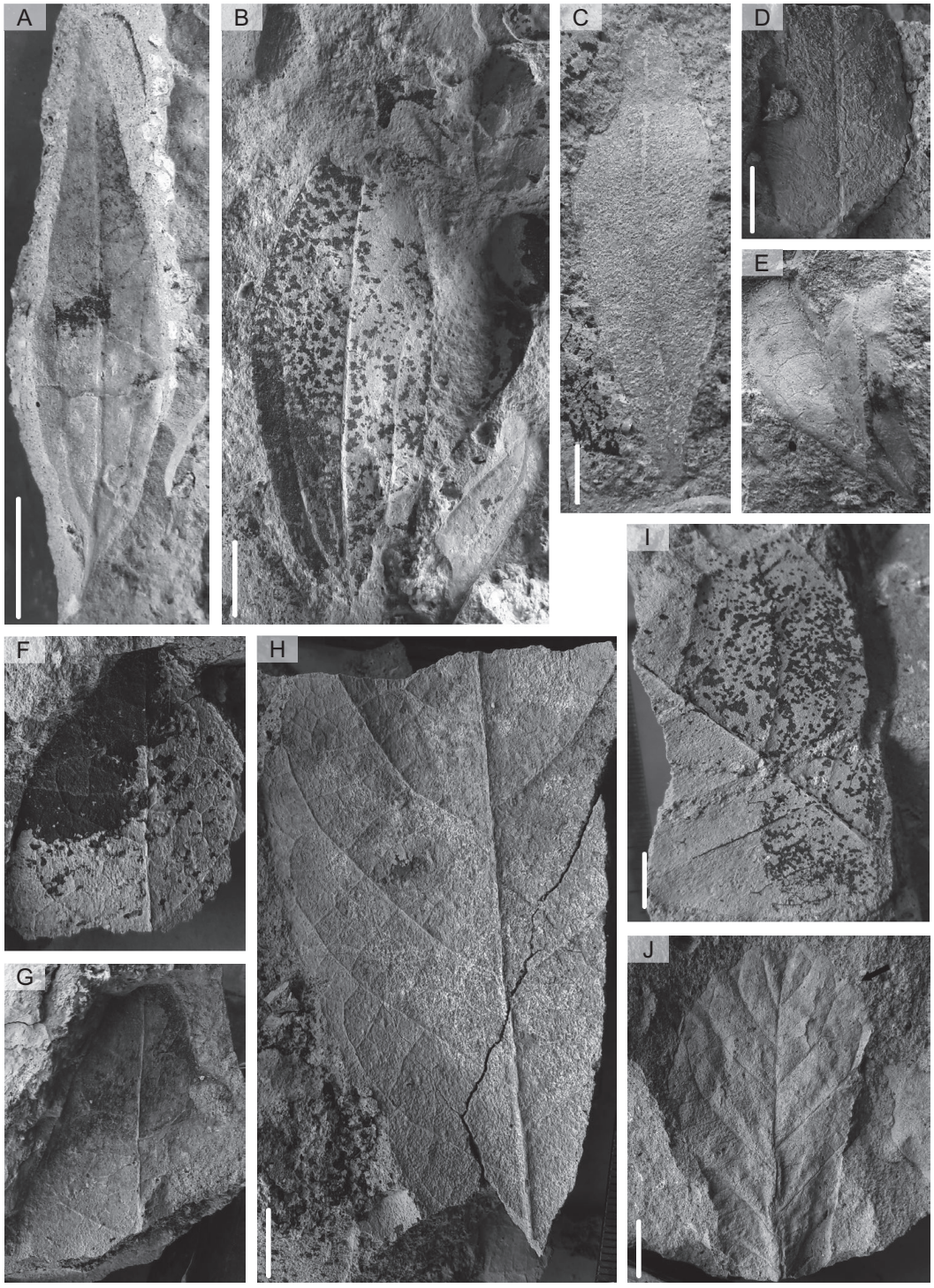

Fig. 7. Plant assemblage from Kamenica nad Hronom 1, scale bar – 10 mm. The studied plant fossil record is housed in the paleobotanical collection of the Slovak National Museum-Natural History Museum in Bratislava (SNM-NHM). **A, B:** *Daphnogene polymorpha* (A. Braun) Ettingshausen. **A —** Complete elliptic leaf with attenuate apex, cuneate base, entire margin and suprabasal acrodromous venation (B 1860). **B —** Incomplete broadly elliptic leaf with attenuate apex, entire margin and suprabasal acrodromous venation (B 1861). **C, D:** *Laurophyllum* sp. 1. **C —** Incomplete oblong to elliptic leaf with cuneate base, entire margin and indistinct secondary brochidodromous venation (B 1862). **D —** Leaf fragment with entire margin and distinct secondary brochidodromous venation (B 1863/1). **E–I:** *Laurophyllum* sp. 2. **E —** Incomplete obovate leaf with emarginate apex, entire margin and distinct brochidodromous secondary venation (B 1864/1). **F —** Incomplete apical part of elliptic or obovate leaf with incomplete short attenuate apex and distinct brochidodromous secondary venation and regular polygonal reticulated venation of higher order (B 1865/1). **G —** Incomplete apical part of elliptic leaf with blunt apex and distinct brochidodromous secondary venation and regular polygonal reticulated venation of higher order (B 1865/2). **H —** Incomplete large elliptic or obovate basal leaf part with distinct brochidodromous secondary venation and regular polygonal reticulated venation of higher order. (B 1863/2). **I —** Incomplete basal leaf part with distinct brochidodromous secondary venation and regular polygonal reticulated venation of higher order (B 1866). **J —** *Ternstroemites* sp., incomplete obovate leaf with simple serrate margin and round teeth (black arrow) (B 1867).

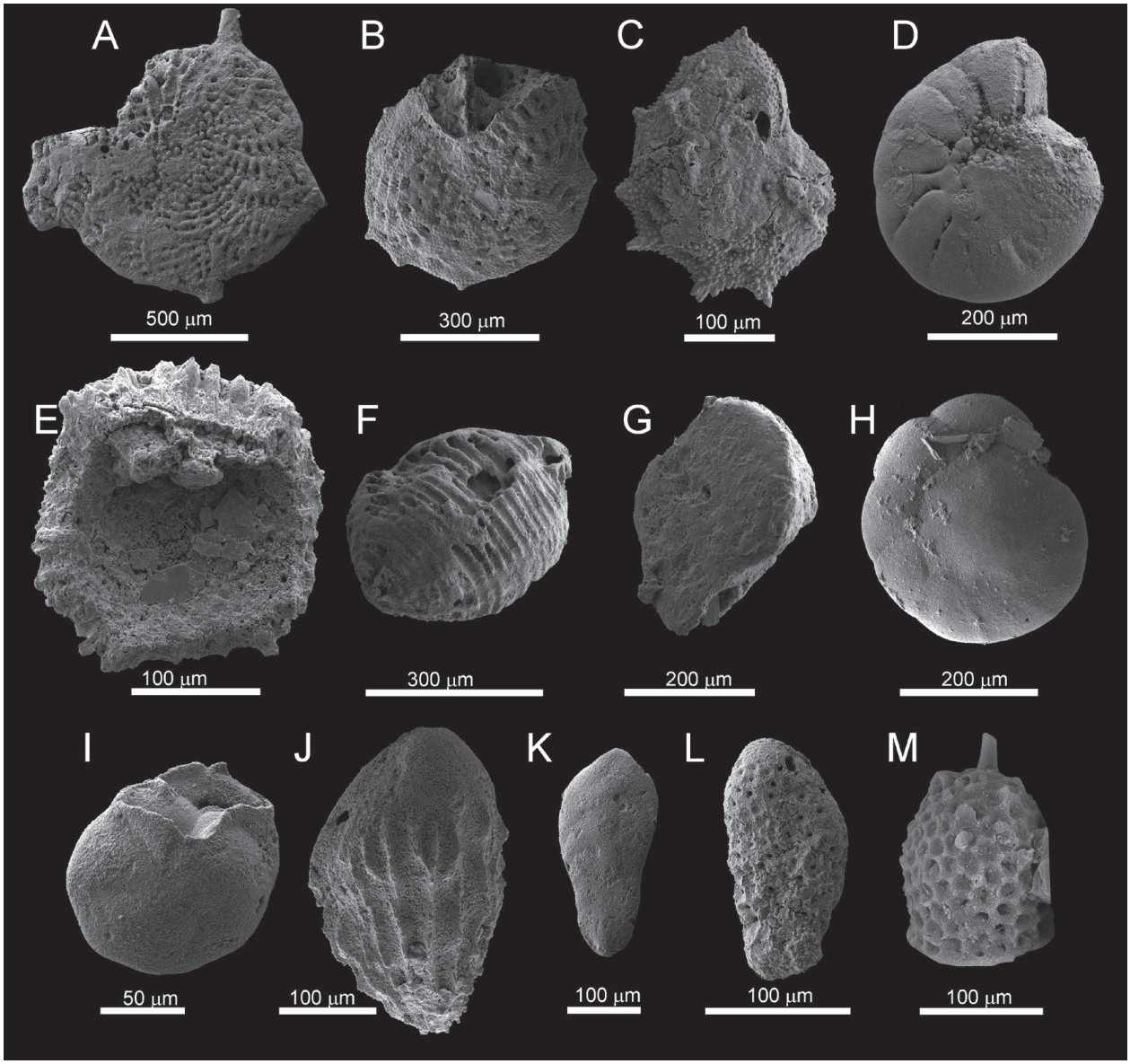

Fig. 8. Foraminifera and radiolaria under the scanning electron microscope. **A** — *Elphidium reginum* (d´Orbigny 1846); Lontov, LON-2. **B** — *Elphidium aculeatum* (d'Orbigny 1846); Lontov, LON-2. **C** — *Elphidium josephinum* (d´Orbigny, 1846); Lontov, LON-2. **D** — *Porosonion* sp.; Lontov, LON-2. **E** — Radiolaria sp. indet; Lontov, LON-1. **F** — *Borelis melo* (Fichtel & Moll 1798); Kamenica nad Hronom 2, KH2-1. **G** — *Cibicides refulgens* Montfort 1808; Kamenica nad Hronom 2, KH2-1. **H** — *Ammonia parkinsoniana* (d'Orbigny 1839); Kamenica nad Hronom 2, KH2-1. **I** — *Cassidulina laevigata* d'Orbigny 1826; Lontov, LON-1. **J** — *Bulimina striata* d'Orbigny in Guérin-Méneville 1832; Lontov, LON-1. **K** — *Bolivina* ex gr. *dilatata* Reuss 1850; Lontov, LON-1. **L** — *Bolivina hebes* Macfadyen 1930; Lontov, LON-1. **M** — Radiolaria sp. indet; Lontov, LON-1.

The **Tlmače** section (Figs. 2, 4, 9A) is divided into two units. The first 10 cm-thick unit is formed by normally-graded conglomerates (up to pebble size clasts; Gcg). These sediments are overlain by a 5 cm-thick red mudstone layer (Fm). Then two beds with normally graded conglomerates follow (Gcg). The lower bed is 45 cm thick (clasts up to 2 cm in diameter) and the upper bed is 50 cm thick (clasts up to 5 cm in diameter). The overlying lithofacies consists of massive coarse-grained sandstone, which is 10 cm thick (Sm). This layer is overlain by 10 cm-thick Gcg lithofacies and then by a 30 cm-thick fossiliferous, volcaniclastic mudstone (Fm; Fig. 9B). Debris follows and the overlying unit is composed of a 70 cm-thick andesite breccia (Fig. 9C), which is covered by recent soil. Andesites with porphyric texture are composed of plagioclase, pyroxene and biotite phenocrysts in microlithic groundmass. Pyroxenes are altered to secondary minerals. Less common biotite contains opacitic rim.

Mudstones (Fig. 4; sample TL-2) are formed especially by volcanic material altered to clay minerals, chloritization is also present. The grains are composed of volcanic lithoclasts, vitroclasts, plagioclase crystalloclast, quartz and biotite. Glauconite and one fragment of spherulite were also found.

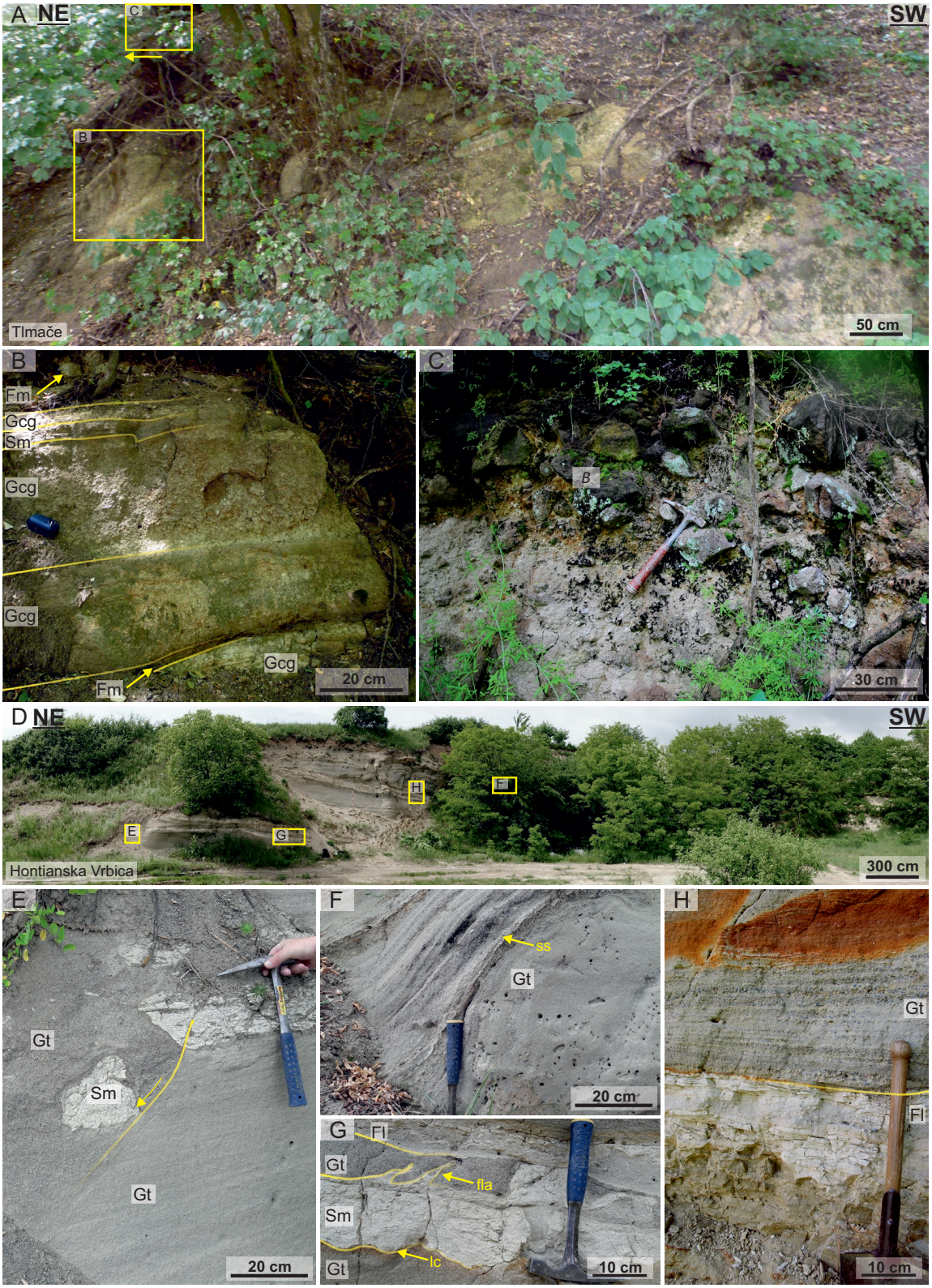

Fig. 9. Photoplate of the Tlmače and Hontianska Vrbica sections. **A** — Overall view of the Tlmače section with marked position of lithofacies details. **B** — Alternation of the normally graded conglomerates with mudstones and massive sandstones (between 0 and 1.5 m from the base). **C** — Andesite conglomerates (between 0 and 0.7 m from the top). **D** — Overall view of the Hontianska Vrbica section with marked position of lithofacies details. **E** — A massive sandstone rip-up clast in a scour filled with trough cross-bedded conglomerates (between 0.4 and 1.2 m from the base). **F** — Detail of the soft-sediment deformation (ss) in trough cross-bedded conglomerates (between 5.2 and 4.9 m from the base). **G** — Massive sandstones limited by load cast structure (lc) at the base and flame structure (fla) at the top (between 0.9 and 1.2 m from the base). **H** — Laminated siltstones overlain by trough cross bedded conglomerates (between 4.3 and 3.6 m from the top). For lithofacies codes and interpretations see Fig. 3.

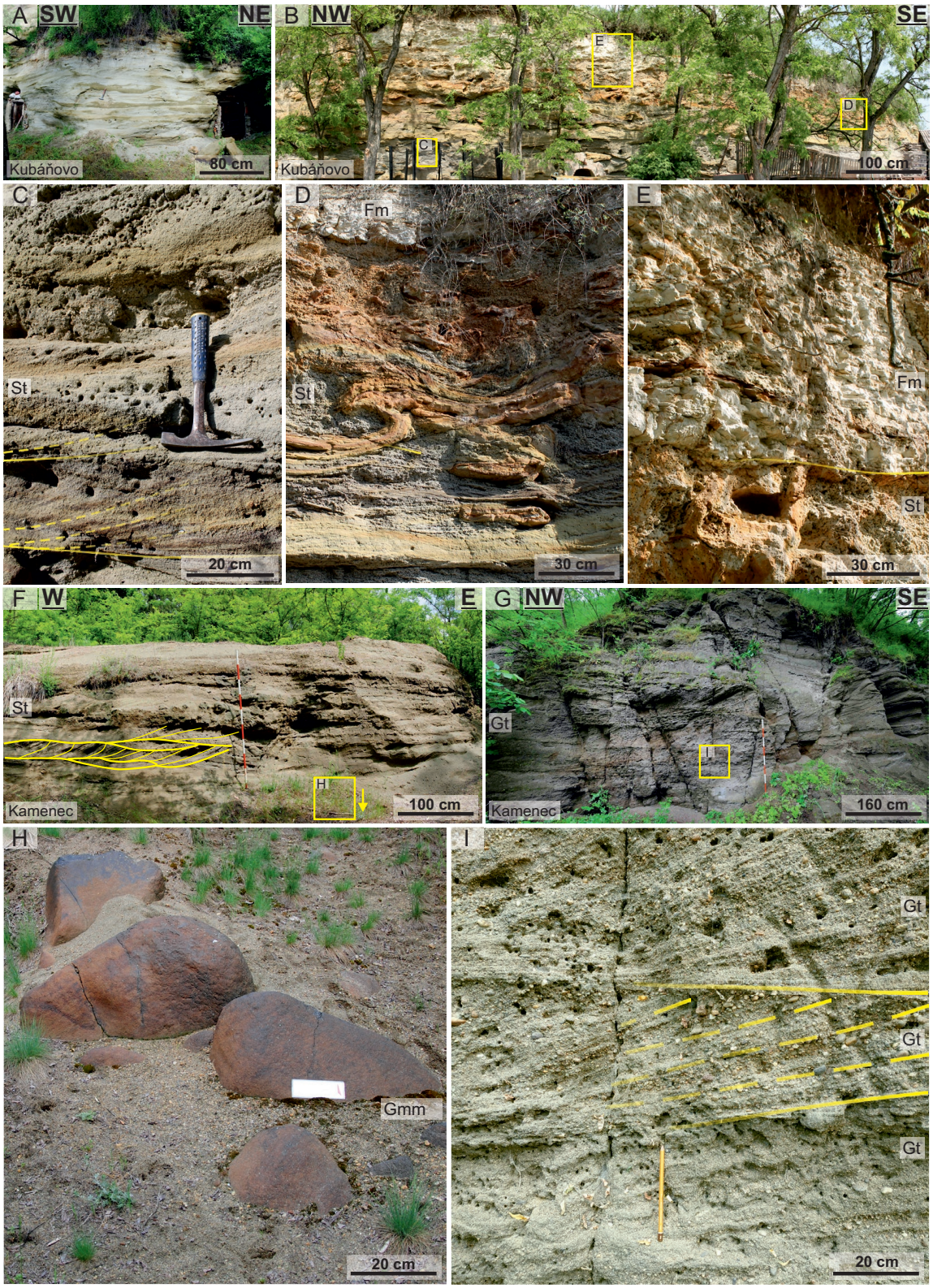

Fig. 10. Photoplate of the Kubáňovo and Kamenec sections. **A–B** — Overall view of the Kubáňovo section with marked lithofacies details. **C** — Trough cross-bedded sandstones (between 1 and 1.9 m from the base). **D** — Trough cross-bedded sandstones with pronounced Liesegang rings (between 4.4 and 5.8 m from the base). **E** — Trough cross-bedded sandstones and overlying siliceous mudstones (between 5.1 and 6.3 m from the base). **F** — The lower part of the Kamenec section composed of trough cross-bedded sandstones with marked lithofacies details (between 1 and 3 m from the base). **G** — Overall view of the uppermost level of the Kamenec section composed of trough cross-bedded conglomerates with marked lithofacies detail (between 5 and 0 m from the top). **H** — Massive conglomerates at the base of the section (between 0 and 1 m from the base). **I** — Detail of the trough-cross bedded conglomerates (between 4.2 and 3.1 m from the top). For lithofacies codes and interpretations see Fig. 3.

Lithoclasts are composed of microlithic glassy groundmass with Pl phenocryst. Matrix is tuffaceous and locally pigmented by ferric oxide. Epiclastic origin is documented by the roundness of some grains, by absence of mafic mineral and by the presence of abundant fossils. Therefore, these sediments can be assigned to volcanic siltstones to mudstones.

The fine-grained conglomerate sample (up to 1.6 cm in diameter; Fig. 4; sample TL-1) consists of gravel grains (61 %), sandy grains (24 %) and lutite fraction (15 %). The conglomerates are composed of andesite clasts, plagioclase, heavy minerals and small amounts of pumice. Pyroxene strongly dominates in the heavy fraction (80.5 %), where both, orthopyroxene (enstatite) and clinopyroxene (diopside) are present. Amphibole (magnesio-hastingsite) and biotite are also observed (Fig. 12A,B; Suppl. Table S2).

The **Hontianska Vrbica** section (Figs. 2, 4, 9D) consists of three lithofacies: the first is represented by trough cross-bedded conglomerates to coarse grained sandstones (Gt), which are normally graded. Rip-up clasts may be present within some beds and were eroded from the following fine-grained lithofacies (Fig. 9E). The second lithofacies is composed of light coloured massive silty sandstones (wacke; Sm), where soft-sediment deformations are present (load cast, flame and pillar structures; Fig. 9F,G). The third type is formed by light coloured laminated siltstones (Fl), which contain mollusc shells, fossil leaves and are bioturbated. The lower part of the section (4.35 m thick) is formed by Gt (bed up to 80 cm), which is intercalated by Sm and Fl lithofacies (up to 15 cm). Clasts reach granule size, apart from the rip-up clasts that reach 30 cm. The formation of these clasts is clearly documented in this part, where a Sm bed is torn into rip-up clasts in a scour and fill structure (Fig. 9E). In the upper part (5 m thick), Gt lithofacies contain pebble size clasts and the maximal thickness of the bed is up to 40 cm. Pillar structures are observed locally. Within this part Fl lithofacies forms a 65 cm-thick unit, which is intercalated by very thin Gt lithofacies (Fig. 9H). Liesegang rings are common in the entire section together with soft-sediment deformations (scour and fill structures). The dip of the cross-beds is generally towards the north to the west and the section terminates with recent soil.

Grain-size analysis from light coloured layers (Fig. 9E,G) shows that the lower layer corresponds to a poorly sorted wacke (75 % sandy fraction, 23 % silt, 2 % clay, sorting= 1.83 phi; Fig. 4; sample HON-1). The overlying light coloured layers correspond to sandy siltstones (21 % sandy fraction, 72 % silt, 7 % clay fraction, sorting=1.78 phi; Fig. 4; sample HON-3). The siltstones are composed of subangular to rounded quartz, feldspar, muscovite grains and biogenic silica remnants (sponge spicules; Fig. 6E). These layers are poor in carbonates (under 0.08 % $CaCO_3$).

The base of the **Kubáňovo** section (Figs. 2, 4, 10A,B) is formed by a 3 m-thick unit of grouped trough cross-bedded sands (St; Fig. 10C) that contain pumice and siliceous mudstone intraclasts of gravel size. Above, a similar 2.5 m-thick lithofacies (St) occurs, with rare intraclasts. Secondary structures are represented by Liesegang rings, ferric and calcareous concretions (Fig. 10D). The dip of these cross-beds is generally towards the south-west (Fig. 4) and thickness of individual beds is up to 15 cm. The section ends with ~10 m-thick siliceous mudstone (Fm) dissected by secondary calcareous and ferric intercalations (Fig. 10E). Within this mudstone rhizoliths and leaves are present, and the section is terminated by recent soil.

The mudstone (Fig. 4; sample KUB-1) contains subangular to rounded silty grains in clay matrix. In mineral composition quartz dominates. Biotite, chlorite, plagioclase, glauconite and carbonized grains are also present. On the basis of the large portion of biogenic silica remnants (sponges, diatoms), these sediments can be identified as biogenic Si-rich to siliceous mudstone (Fig. 6G,H).

The lowermost part of the **Kamenec** section (Figs. 2, 4, 10F,G) begins with large andesite boulders (Gmm; Fig. 10H), which reach 1 m in diameter. Above, 2 m-thick trough cross-bedded sandstones are present (beds are up to 40 cm; St; Fig. 10F). Sandstones are coarse-grained with transition to conglomerate (up to 6 cm) at the base of beds. The dip of these cross-beds is towards the north-north-west. The next lithofacies is composed of 130 cm-thick trough cross-bedded conglomerate (up to pebble size clasts; Gt). This part of the section is intersected by debris. The second part is composed of 2.2 m-thick St lithofacies, which are intercalated by tuffaceous mudstone (F). However, this part of the section is poorly preserved and is followed by second debris. The third part is ~5 m thick and is composed of Gt lithofacies with normal gradation (beds are up to 60 cm; Fig. 10G,I). The dip of the cross-beds is generally towards the north and the section is terminated by recent soil.

The **Zbrojníky** section (Figs. 2, 4, 11A) is formed by well sorted grains of sand and gravel fraction (up to pebble size), which can be divided into three lithofacies: the first is composed of sands with low angle lamination (Sla; Fig. 11C); the second lithofacies consists of trough cross-bedded gravels with clasts up to pebble size (Gt); the third is formed by trough cross-bedded sands (St). The overall cross-bed dip is polymodal. The Sl lithofacies dominate in the lower part of the section (average thickness 40 cm) and alternate with Gt and St lithofacies. The middle part is dominated by St lithofacies (up to 115 cm). The upper part is formed by Gt lithofacies (up to 100 cm) with abundant muddy rip-up clast at the base of this unit (Fig. 11B). Liesegang rings are common in the entire section, rare ferric concretions are also observed. A large fossil mammal bone fragment was found in debris (Fig. 11D). The section is topped by recent soil.

The **Podlužany** section (Figs. 2, 4, 11E) consists of 4 partial profiles differing in horizontal and vertical lithological development. The lowermost part of the section consists of 50 cm-thick trough cross-bedded sandstones, which are poorly sorted (St). The next lithofacies is 15 cm thick and is composed of fossiliferous intraformational conglomerate (Gt) formed by mudstone rip-up clasts. The clasts contain rhizoliths and large mammal bone fragments (Fig. 11F).

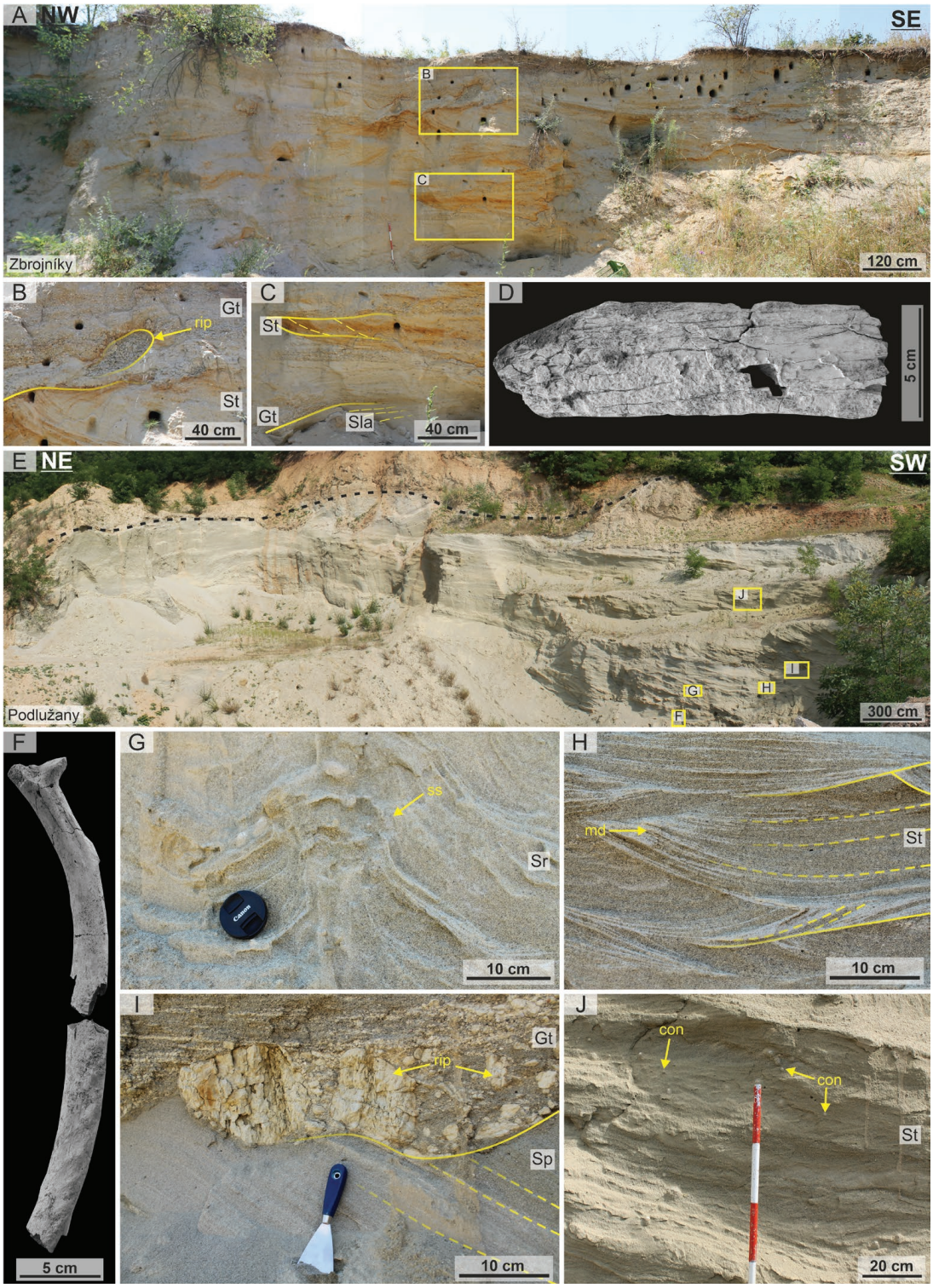

Fig. 11. Photoplate of the Zbrojníky and Podlužany sections. **A** — Overall view of the Zbrojníky section with marked position of lithofacies details. **B** — Trough cross-bedded sandstones overlain by trough cross bedded conglomerates with the rip-up clasts (rip) at the base (marked with arrow; between 1.3 and 0.2 m from the top). **C** — Detail with marked low-angle laminated sandstones, trough cross-bedded sandstones and conglomerates (between 0.4 and 1.6 m from the base). **D** — Large mammal bone fragment found in the debris. **E** — Overall view of the Podlužany section with marked position of lithofacies details. The black dash lines mark the boundary between Miocene and Quaternary deposits. **F** — Large mammal bone fragment (*Rhinocerotidae* indet., determined by Martin Sabol) found in rip-up clast at the base of trough cross-bedded conglomerates (~0.65 m from the base). **G** — Arrow shows soft-sediment deformation (ss) in ripple cross-laminated sandstones (between 1.3 and 1.7 m from the base). **H** — Trough cross-bedded sandstones with mud drape structures (md; marked by arrow; between 2.4 and 2.7 m from the base). **I** — Planar cross-stratified sandstones and overlying trough cross-bedded conglomerates with rip-up clasts (rip) marked by an arrow (between 3.6 and 4.1 m from the base). **J** — Arrow marks concretions (con) observed in trough cross-bedded sandstones (between 7.1 and 8.5 m from the base). For lithofacies codes and interpretations see Fig. 3.

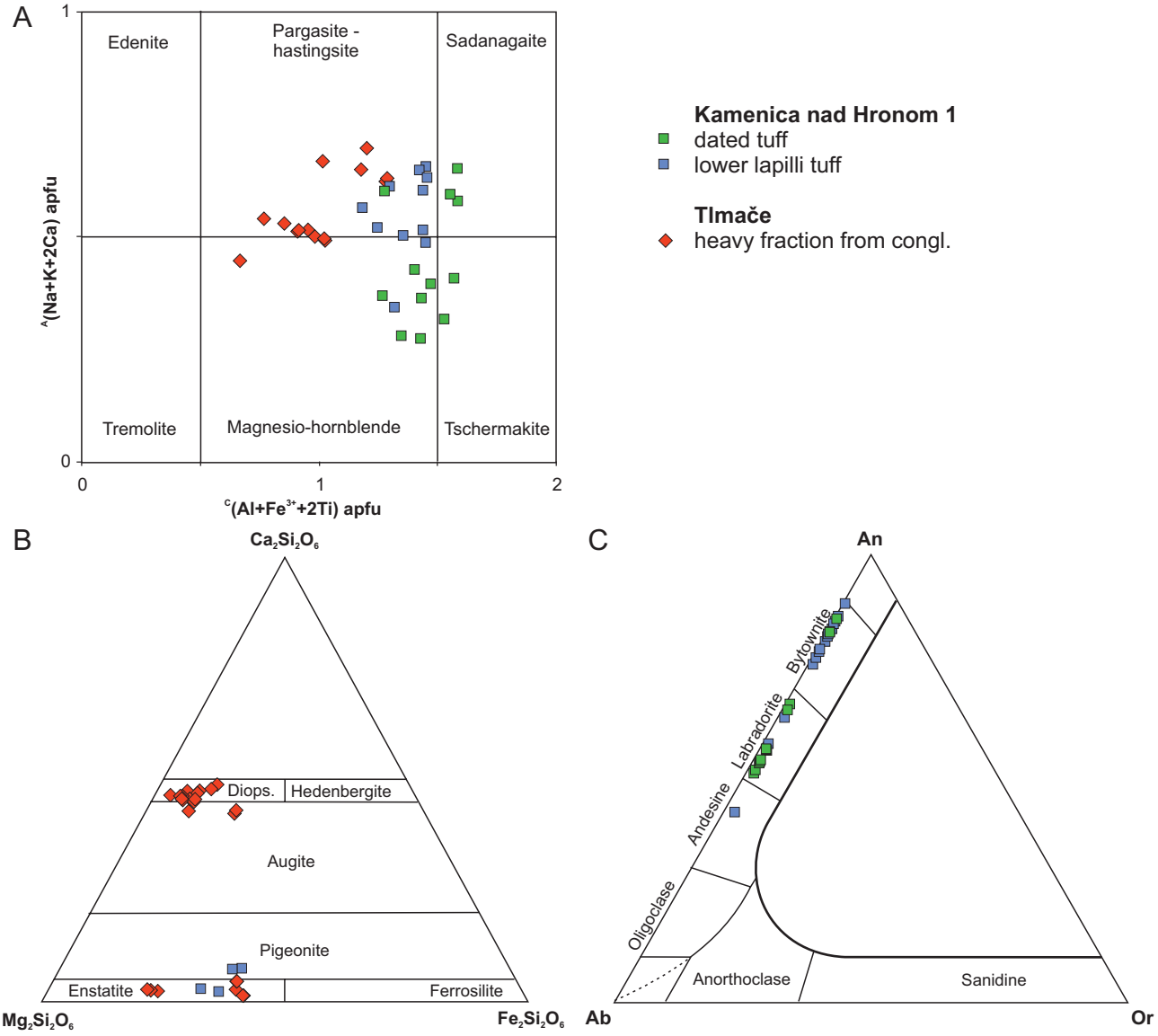

Fig. 12. Ternary plots. **A** — Composition of amphiboles in normally graded conglomerates (the Tlmače section), in lower lapilli tuffs and in coarse dated tuffs (the Kamenica nad Hronom 1 section). **B** — Composition of pyroxenes in lower lapilli tuff from the Kamenica nad Hronom 1 section and in normally graded conglomerates from the Tlmače section. **C** — Composition of feldspars in lower lapilli and dated coarse tuff from the Kamenica nad Hronom 1 section.

The overlying 120 cm-thick unit consists of ripple cross-laminated sandstones with small rip-up clasts that decrease upwards (Sr). In the upper 80 cm-thick part, the Sr lithofacies is laterally affected by soft-sediment deformation (pillar structures, Fig. 11G). Higher up, a 120 cm-thick St unit with mud drapes structures follows (Fig. 11H). The next 60 cm-thick bed is composed of planar cross-stratified sand (Sp). An erosional contact follows, and an 80 cm-thick Gt layer occurs (Fig. 11I). The grain size of rip-up clasts decreases upwards. Another erosional boundary follows and a 140 cm-thick St lithofacies is present. At the base of this unit rip-up clasts are very abundant. Higher up, 70 cm-thick debris is present, which is followed by a discontinuous St lithofacies (~390 cm). Within the lower part soft-sediment deformations (pillar structures) and calcareous concretions are observed (Fig. 11J). The overall dip of the cross-beds is towards the south. The section is topped by loess.

Discussion

Local-scale discussion

Stratigraphic ranking

The mollusc species (*Ancilla glandiformis, Cerithium vulgatum, Linga columbella)* and calcareous nannoplankton species (*Discoaster* cf. *exilis*), indicate that the sandstones from **KH2** section were deposited during the late Badenian (early Serravallian). This inference is in accord with previous studies

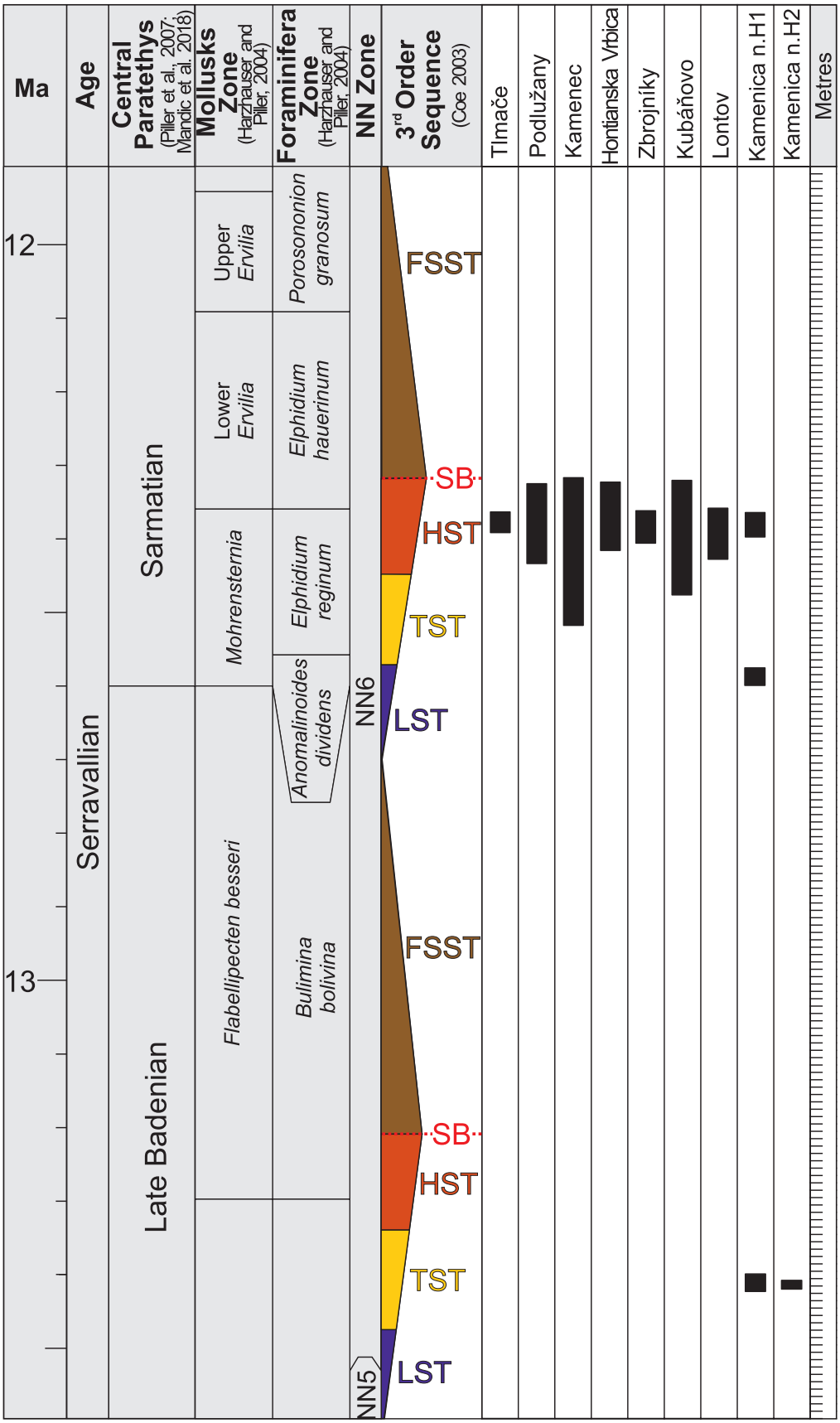

Fig. 13. Chronostratigraphy, biostratigraphy and sequence stratigraphy of the studied sections (timing of the regression–transgression triangles was adopted from Hohenegger et al. 2014).

that documented *Amphistegina* sp., *Pecten besseri*, *Amussium denudatum*, *Costellamussiopecten cristatus, Codakia leonina*, *Vaginella* sp. *Cerithium* sp., *Turritella* sp., *Dentalium* sp., *Brissopsi*s sp. and elements of NN6 zone from sections near KH2 (Seneš et al. 1962; Vaškovský et al. 1982). The volcanic conglomerates at the base of the **KH1** can be assigned to the lower Badenian (Langhian; Vaškovský et al. 1982; Bezák et al. 2009). Nevertheless, the overlying tuff breccia and lapilli tuff do not yield any index fossils, so their age is inconclusive. However, sponge spicules indicate (sample KH1-1 from Tb) a subaquatic environment and allow correlation with the late Badenian fossiliferous sandstones from KH2 that also contain abundant sponge spicules (samples KH2-1 and KH2-2). We thus set the Badenian/Sarmatian boundary on the top of the lapilli tuff (KH1-2 sample; Fig. 4). The coarse tuff (Figs. 4, 5B, 13) from the upper part of the KH1 section is dated to 12.56±0.10 Ma by Ar/Ar (Sant et al. 2020) and according to Mandic et al. (2018) can be assigned to the earliest Sarmatian (Serravallian). In the **Lontov** section, the early Sarmatian stratigraphic assignment is based on foraminifera (*Elphidium reginum, E. josephinum, E. macellum*, *Schackoinella imperatoria*, *Ammonia parkinsoniana, A. viennensis, Bolivina antiqua, B. dilatata, Ciperoella ciperoensis, Globorotalia transsylvanica, Porosononion martkobi*) and molluscs (*Cerithium rubiginosum*, *Granulolabium bicinctum*, *Duplicata duplicate*, *Euspira helicina sarmatica,* and *Vitta picta*). Calcareous nannoplankton species support this lower Sarmatian assignment as they, also include taxa typical of the NN6 Zone (Martini 1971; *Braarudosphaera bigelowii parvula*, *Calcidiscus leptoporus*, *C. pataecus*, *Coccolithus miopelagicus*, *Helicosphaera walbersdorfensis*, *Helicosphaera wallichii, Holodiscolithus macroporus, Reticulofenestra pseudoumbilicus* > 8 μm, *Rhabdosphaera sicca).* Apart from the autochthonous taxa, the sample also includes index fossils of the NN4 and NN5 Zone (*Helicosphaera ampliaperta, Sphenolithus heteromorphus*) that are probably reworked from older strata. Similar foraminifera (*Elphidium reginum*, *E. aculeatum, E. macellum, E. fichtelianum, Anomalina badenensis, Ammonia beccarii*) and mollusc assemblages (*Gibbula* aff. *angulata, Calliostoma* sp*., Acteocina lajonkaireana, Musculus sarmaticus, Abra reflexa, Loripes dentatus, Ervilia* sp*., Cardium* sp.) were previously reported by Nagy et al. (1998).

The **Tlmače** section may be associated with the early Sarmatian (Serravallian), on the basis of the mollusc assemblage (*Rissoa* sp., *Mohrensternia* sp., *Abra* sp., *Inaeqnicostata politioanei suessiforme*, *Limnocardium* sp., *Loripes* sp. and *L.s* aff. *dujardini*). The **Hontianska Vrbica** section is also assigned to the early Sarmatian stage, which is confirmed by the determined mollusc assemblage (*Cerastoderma* cf. *latisulcum* and *C. latisulcum nexingense*). This study has not documented any biostratigraphic indicators in the **Kubáňovo** section, however the Sarmatian foraminiferal assemblage was reported by Nagy et al. (1998; *Ammonia beccarii*, *Elphidium flexuosum flexuosum*, *E. macellum,* and *Protelphidium bogdanowicz*). The **Kamenec, Zbrojníky** and **Podlužany** sections do not contain any biostratigraphic markers but can be correlated with the Sarmatian deposits at other sections in the Želiezovce Depression on the basis of similar lithology and proximity.

Badenian paleoenvironmental conditions

The KH2 section (Figs. 3, 4, 5A–E, 13) may be interpreted as a wave and possibly tide dominated late Badenian rocky shore, which is indicated by clast-supported gravels (Gcm facies) and fossiliferous faintly laminated sandstones (Sm). The mollusc assemblage at this section also indicates the infralittoral zone (*Alvania costata*, various rissoids, and *Cerithium vulgatum,* which were redeposited from the rocky litoral zone; Senešová 1980). The Gcm conglomerates from KH2 are well rounded, in contrast to the Gmm conglomerates from the lower part of the KH1 section, which are angular and were interpreted as pyroclastic flows and lahars (Bezák et al. 2009). The KH2 deposits are probably synchronous with the tuff breccia and lower lapilli tuff (Tb, Lt; Németh & Martin 2007) from the KH1 section, which contain indicators of subaquatic deposition (sponge spicules and pigeonite) and major erosional surface at the top of the Lt facies.

Sarmatian paleoenvironmental conditions

The upper part of the KH1 (Figs. 4, 5A–D, 13) is characterized by several tuff layers and mudstones (Lt, Ct, Fm; Németh & Martin 2007), which alternate with conglomerates (Gg, Gmg; Miall 2006) that can be interpreted as terrestrial debris flows. Continental subtropical conditions are inferred from the plant assemblage found at the top of the coarse tuff (Ct; Fig. 5B). This association is characterized by common thermophilous evergreen elements (Fig. 7; *Daphnogene polymorpha, Laurophyllum* sp. and *Ternstroemites* sp.), which usually grow in broad-leaved evergreen forests such as modern woodlands of SE China (e.g., Wang 1961; Teodoridis et al. 2011).

The **Lontov** section (Figs. 4, 5F, 13) includes rhythmic laminated (Rossi et al. 2017) sandstones and siltstones (Sl, Fl) together with fossiliferous planar cross-stratified conglomerates (Gp). These lithofacies were deposited from suspension and by traction, possibly accounting for Karpatian and Badenian (Burdigalian and Langhian) microfossils (Sl, Fl, Gp; Miall 2006). They can be interpreted as a tide dominated Sarmatian (Serravallian) coast, developed on a coarse-grained delta top. Previous studies also describe normally graded sandstones, load casts and current ripples as well as synsedimentary folds, which were interpreted as lower shore-face deposits (Nagy et al. 1998). This is not in contradiction with the interpreted environment.

The graded conglomerates (Gcg) of the **Tlmače** section (Figs. 4, 9A,B, 13) were probably deposited by traction and are interpreted as an alluvial fan. While the fossiliferous muddy intercalations (Fm) may indicate short break in the dynamic sedimentations and point to deposition from suspension, connected to ephemeral lakes with marine ingressions.

The overall paleoenvironment can be linked to a topset and foreset of a coarse-grained delta (Nemec 1990; Nichols 2009). This is consistent with the originally mentioned littoral wave dominated coast described by Konečný et al. (1998) and Nagy et al. (1998).

The trough cross-bedded conglomerates (Gt) from the **Hontianska Vrbica** section (Figs. 4, 9D–H, 13) were deposited by traction and according to Miall (2006) can be interpreted as remnants of channel fills. The intercalating sandstone (Sm) yields soft-sediment deformation, which indicates rapid deposition, subsequent liquefaction and fluidization connected mainly with the fluvial environment (Lowe & LoPiccolo 1974; Neuwerth et al. 2006; Rossi et al. 2017). The fossiliferous laminated siltstones (Fl) were deposited from suspension and point to episodes with marine ingressions. Overall, these lithofacies can be placed on a fluvial dominated and tide influenced delta top (Rossi et al. 2017). The deltaic conditions were also recognized by Nagy et al. (1998), who linked the paleoenvironment with a foreset-bottomset boundary. However, the erosion boundaries and rip-up clasts formed by Sm and Fl, point to much shallower conditions compatible with river channel incision. While the Fl lithofacies have enough clay particles for cohesive behaviour, the Sm lithofacies do not. But based on the presence of mollusc casts, early diagenetic carbonization was responsible for cohesion of this lithofacies, which allowed formation of rip-up clasts. Macroflora from the siltstones (*Picea* sp., *Salix tenera, Betula macrophyla, Zelkova zelkovaefolia, Phragmites oeningensis*, *Cyperites* sp.) indicate temperate climate conditions during the early Sarmatian (Serravallian; Nagy et al. 1998).

The cross-bedded sandstones with occasional rip-up clasts from the **Kubáňovo** (Figs. 4, 10A–E, 13) section (St) were most likely deposited by traction currents and may be interpreted as sinuous-crested and linguoid dunes. The siliceous mudstones (Fm) were deposited from suspension and based on foraminiferal content, ephemeral lakes with marine ingressions can be assumed. Previously, hydroplastic deformations in the upper part of the sandstones were interpreted (Nagy et al. 1998), however this study observed that the cross-bed laminas pass straight through the assumed hydroplastic deformations (Fig. 10D). This rather points to secondary origin of these structures, which are represented by secondary Liesegang features and ferric concretions. The documented lithofacies indicate a fluvial environment covered by marine ingressions. In the past, an estuarine environment was assumed (Nagy et al. 1998), and the present study does not contradict this view. Based on the correlation with other described sections, a transition from fluvial dominated coarse-grained delta to estuarine environment may be assumed.

The boulders (Gmm) at the base of **Kamenec** section (Figs. 4, 10F–I, 13) can be interpreted as plastic debris flow. Above, St and Gt lithofacies were deposited by traction and point to sinuous-crested and linguoid dunes developing in channel fills (Miall 2006). Intercalations of F lithofacies were deposited from suspension and are interpreted as abandoned channels or alluvial plain deposits. Overall, such an environment can be interpreted as fluvial dominated and may be placed on a coarse-grained delta top. In a previous study, a tide influenced deltaic environment was suggested, on the basis of herringbone structures (Nagy et al. 1998). However, this can be excluded, since all cross-beds are unidirectional and dip north.

Trough cross-stratified sands and conglomerates (St, Gt) from the **Zbrojníky** section (Figs. 4, 11A–D, 13) were deposited by traction and can be interpreted as sinuous-crested and linguoid dunes developing in river channels. Muddy rip-up clasts at the base of Gt may indicate redeposition of flood plain material into the base of the channels. Sandstones with faint low angle lamination (Sla) can by interpreted as scour fills or supercritical flow deposits. Generally, the described lithofacies point to a fluvial environment, and this is supported by correlation with other sections.

Mudstone rip-up clasts from the **Podlužany** section (Figs. 4, 11E–J, 13) form the Gt lithofacies and indicate redeposition from the flood plain to the base of channels. These intraformational conglomerates (Gt) were deposited by traction transport in channel fills. This can be supported by presence of rhizoliths and large mammal bone fragments in the rip-up clasts (*Rhinocerotidae* indet., determined by Martin Sabol; Fig. 11F). The erosional contacts at the base of Gt suggest amalgamation of channel bodies in a channel-belt (Fig. 11G). The St, Sp lithofacies indicate traction transport and can be interpreted as 2D and 3D dunes evolving in a channel. The sandy Sr lithofacies suggest deposition in lower flow regime. Furthermore, Sr with pillar structures (soft-sediment deformation connected with water escape; Fig. 11G) are typical for environments with high depositional rates and the end of high energy events that mainly occur in fluvial and tidal environments (Rossi et al. 2017). Overall, the presence of fluvial channel belt facies is mainly supported by unidirectional cross-beds, erosional surfaces and rip-up clasts. Therefore, the association of lithofacies points to an environment dominated by fluvial and effected by tidal processes. Such an environment may have developed within a delta plain.

Regional-scale discussion

The late Badenian rocky shores have a transgressive character (TST and/or HST) and are mainly developed in the southern segment of the Želiezovce Depression. Such transgressive settings were also documented by sea-grass meadows from the close by ŠO-1 well (Chľaba) located near Štúrovo (Holcová et al. 2019) and might also be preserved in the central part of the Želiezovce Depression as well, where Kováč et al. (2018) described coastal plains. Similar transgressive conditions are reported also from the Vienna Basin, where fully marine, barrier-lagoon systems were deposited during the late Badenian (Hyžný et al. 2012; Ruman et al. 2017; Harzhauser et al. 2018). In the Carpathian Foredeep, late Badenian transgressive sediments can be connected with the Badenian salinity crisis (Śliwiński et al. 2012). The deposition is expressed by evaporites followed by normal marine sediments (Śliwiński et

al. 2012; Peryt et al. 2014). This normal marine environment probably reached all the way to the North Croatia Basin where the late Badenian is represented by lagoonal to near-shore settings (Bakrač et al. 2010). The erosion and/or non-deposition during the latest Badenian was already suggested by older studies in the Danube Basin (Seneš et al. 1962; Vaškovský et al. 1982), and the extremely small thickness of the upper Badenian deposits at KH1 indicates that gap is a major feature also in the studied marginal sections. Erosion connected with tectonics and/or with lower 4th–6th order cycles cannot be excluded.

The earliest Sarmatian deposition is represented only by terrestrial tuffs, dated to 12.56±0.10 Ma by $^{40}Ar/^{39}Ar$ method (Sant et al. 2020). The terrestrial conditions during this time indicate that the sea level did not yet reach the shelf, which can be associated with the lowstand system tract at the beginning of the Sarmatian transgression. Subtropical conditions continue up to this time, as is indicated by the plant assemblage from the dated tuffs (Fig. 7).

Subaquatic deposition starts again in the early Sarmatian in a tide influenced deltaic environment (Fig. 14). In general, the delta system seems to be prograding from the east forming a large fan body spanning from the north towards the south (Fig. 14). A good recent day example of such a deltaic system can be found in the Copper River delta (Alaska, USA; Rossi et al. 2017), since it has similar dimensions and is composed of comparable lithofacies. This progradation can be connected with the Sarmatian highstand system tract (HST). Based on lithological composition, the deltaic conditions were also suggested by the previous studies (Seneš et al. 1962; Nagy et al. 1998). The delta entered the central part of the Želiezovce Depression, as is documented by early Sarmatian shallow marine sandy deposits recorded in several wells (Seneš et al. 1962; Biela 1978; Vaškovský et al. 1982; Nagy et al. 1998; Kováč et al. 2018). Good stratigraphic correlation between these wells and studied sections can be established with the help of *Ervilia dissita* bivalves from the Modrany-1 (depth ~1000–1100 m) and from the Dubník-1 wells (depth ~1250–1300 m; Kováč et al. 2018). This species is assigned to the lower and upper *Ervilia* Zone connected with early Sarmatian transgression (late TST and HST; Harzhauser & Piller 2004). This agrees with the interpreted progradation of facies. Evidence for tide and fluvial influence can be supported by alternation of trough cross-bedded facies (Podlužany, Kamenec, Hontianska Vrbica, Zbrojníky, Kubáňovo) with rhytmically laminated strata (Lontov, Hontianska Vrbica). Further support for tidal affects can be derived from the rare presence of mud drape structures (Podlužany). Two types of siliceous mudstones were observed. The first type includes marine fossils and supports the presence of marine ingressions entering from the nearby coast (Kubáňovo, Hontianska Vrbica, Lontov). The second type is non-marine and is interpreted as flood plain mud (Podlužany, Kamenec, Zbrojníky). Both mudstone types contain relatively large amounts of biogenic silica (sponges, diatoms). This can be related to the alteration and dissolution of volcanic glass (sourced from the neighbouring

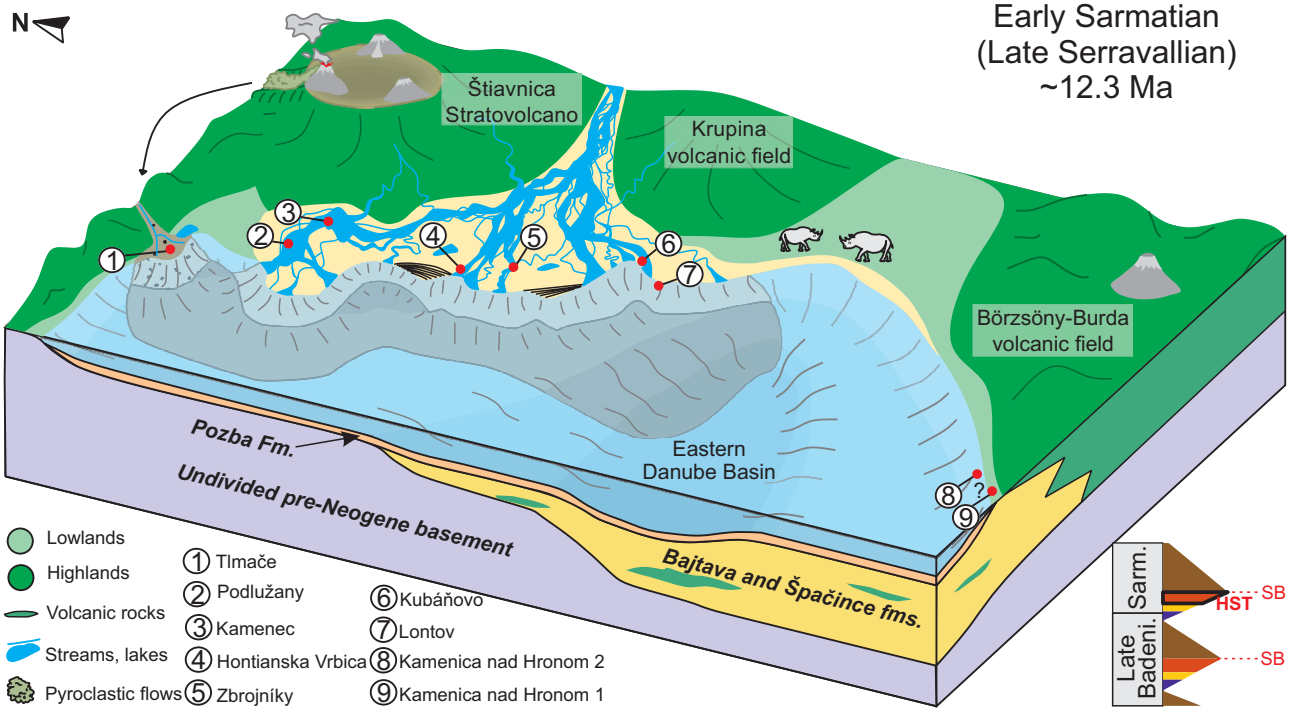

Fig. 14. Block diagram depicting the depositional environment at the eastern margin of Danube Basin during the early Sarmatian (~12.3 Ma, late Serravallian; HST) stage. Timing of the regression-transgression triangles was adopted from Hohenegger et al. (2014). Sequence stratigraphic concept follows Coe (2003).

volcanic fields) into the environment, which later allowed the sponges and diatoms to precipitate their skeletons. The fossil leaves association from this time indicates a climatic turnover to temperate conditions without subtropical elements (Nagy et al. 1998). On the contrary, the northernmost coastline of the depression is formed by alluvial fan to fan delta deposits, triggered and derived from the nearby Štiavnica stratovolcano. The coarse-grained deposition was sporadically interrupted by marine ingressions (Tlmače). These sediments of the Želiezovce Depression may be assigned to the early Sarmatian, based on the absence of the late Sarmatian *Porosononion granosum* zone (Fig. 13) in all sections and reviewed wells. This was already suggested, based on lithostratigraphy, in older regional survey reports (Seneš et al. 1962; Vaškovský et al. 1982; Nagy et al. 1998). The following late Sarmatian erosion and/or non-deposition can be linked with FSST. However, erosion due to lower order cycles or regional tectonics cannot be excluded.

Within the Danube Basin the thickness of the Sarmatian sediments in the central part of the Želiezovce and in Blatné depressions (~300–500 m; Rybár et al. 2016) is relatively low. On the other hand, the thickness of Sarmatian sediments is much higher in the neighbouring Komjatice, Gabčíkovo (~1200–2300 m, Vráble-1 well; Šarinová et al. 2018) and Rišňovce depressions (~1800–3000, Ripňany-1 well; Fordinál & Elečko 2000). The much higher sediment thickness relates to the Sarmatian tectonic opening associated with formation of a large accommodation space. This led to a shift of the deposition from Želiezovce towards the Komjatice and Gabčíkovo depressions. From this point of view a deep water Sarmatian environment also needs to be considered. Therefore, shelf-break slope to stable submarine platform settings can be expected (classification according to Patruno & Helland-Hansen 2018).

The Sarmatian transgression is present in many other basins of the Central Paratethys. The best example can be drawn from the Vienna Basin and the Styrian Basin, where the lower Sarmatian is strongly transgressive (Harzhauser & Piller 2004; Piller & Harzhauser 2005), as is indicated by non-deposition and erosion on the basin margins, accompanied by minor gravels deposited during the Sarmatian LST (Harzhauser & Piller 2004). They are followed by more than 1000 m-thick marls (mainly tidal flats) connected to retrograding Sarmatian TST, which pass to prograding HST gravels. On the other hand, in the Carpathian Foredeep, ~1000 m-thick Sarmatian deltaic complexes (Oszczypko-Clowes et al. 2012) appeared after evaporite and normal marine late Badenian deposition (Śliwiński et al. 2012). In the southern Central Paratethys, shallow marine Sarmatian sediments are also present. In the Drava and Sava depressions, both lower Sarmatian gravity sediments and late Sarmatian shallow water deposits are observed (Pavelić 2001, 2005; Pavelić & Kovačić 2018). Eastward the Sarmatian sediments of the Borod Depression consist of a prograding shallow marine sequences also linked with the Sarmatian transgression (Filipescu et al. 2014). In the southernmost part of the Central Paratethys (Banat Basin), the Sarmatian deposits were probably eroded and the Badenian stratum is directly overlain by Pannonian sediments (Radivojević et al. 2010). In general, early Sarmatian environments point to transgressive settings connected with shallow water conditions.

Conclusions

The late Badenian–Sarmatian (Serravallian) deposition in the Želiezovce Depression of the Danube Basin can be divided into three distinct intervals. The late Badenian rocky shore on the southern margin is formed by massive sandstones and conglomerates. This interval can be associated with the transgressive and/or highstand system tract of the late Badenian stage. A gap in the stratigraphic record, associated with the late Badenian falling stage system tract is inferred. The terrestrial earliest Sarmatian tuffs (12.56±0.10 Ma; $^{40}Ar/^{39}Ar$) can be linked with the beginning of the Sarmatian transgression (lowstand system tract). Their presence indicates that the sea level did not yet reach the shelf. The fossil plant assemblage shows that subtropical conditions prevailed during this time. During the early Sarmatian, a tide influenced deltaic environment evolved in the north. This is indicated by trough cross-bedded facies together with rhythmic laminated strata. The fluvial dominated deltaic facies document progradation towards the basin and are connected with the Sarmatian highstand system tract. During this period a climatic turnover from subtropical to temperate conditions took place, as is confirmed by the fossil leaf association. Sediments of the late Sarmatian were not recorded in this depression because of inferred erosion and/or non-deposition probably linked with the Sarmatian falling stage system tract. However late Sarmatian sedimentation took place in the newly opened Komjatice and Gabčíkovo depressions.

Acknowledgments: This study was supported by the Slovak research and development agency under the contracts No. APVV-16-0121, APVV-15-0575, APVV SK-AT-2017-0010 and grant UK/93/2020. This study was partly supported by the grant projects of GAČR No. P18-25057S and of Charles University, Prague, Progres Q17 (VT). Special thanks go to Tomáš Klučiar and Karin Sant for their participation, help and comments during the field work. Our thanks also go to Oleg Mandic, Mathias Harzhauser and Radoslav Biskupič for consultation on mollusc taxonomy. Above all, we would like to thank our editor and reviewers for guidance and insightful comments.

References

Bakrač K., Hajek-Tadesse V., Miknić M., Grizelj A., Hećimović I. Kovačić M. 2010: evidence for Badenian local sea level changes in the proximal area of the North Croatian Basin. *Geologica Croatica* 63, 3, 259–269.

Bałuk W. 1975: Lower Tortonian Gastropods from Korytnica, Poland, Part 1. *Palaeontologia Polonica* 32, 1–186.

Bałuk W. 1995: Middle Miocene (Badenian) gastropods from Korytnica, Poland; Part II. *Acta Geologica Polonica* 45, 153–255.

Bałuk W. 1997: Middle Miocene (Badenian) gastropods from Korytnica, Poland; Part III. *Acta Geologica Polonica* 47, 1–75.

Bałuk W. 2006: Middle Miocene (Badenian) gastropods from Korytnica, Poland; Part V Addenda et corrigenda ad Prosobranchia. *Acta Geologica Polonica* 56, 177–220.

Bezák V., Biely A., Broska I., Bóna J., Buček S., Elečko M., Filo I., Fordinál K., Gazdačko Ľ., Grecula P., Hraško Ľ., Ivanička J., Jacko sr. S., Jacko jr. S., Janočko J., Kaličiak M., Kobulský J., Kohút M., Konečný V., Kováčik M. (Bratislava), Kováčik M. (Košice), Lexa J., Madarás J., Maglay J., Mello J., Nagy A., Németh Z., Olšavský M., Plašienka D., Polák M., Potfaj M., Pristaš J., Siman P., Šimon L., Teťák F., Vozárová A., Vozár J. & Žec B. 2009: Explanatory notes to geological map of Slovak Republic 1:200,000. *State geological institue of Dionýz Štúr*, Bratislava, 1–534 (in Slovak with English summary).

Biela A. 1978: Deep wells in the covered regions of inner Western Carpathians. Regional geology of Western Carpathians. *State geological institue of Dionýz Štúr*, 1–224 (in Slovak).

Boggs S. 2006: Principles of sedimentology and stratigraphy. *Pearson Prentice Hall*, Upper Saddle River, New Jersey, 1–661.

Boltovskoy E. & Wright R. 1976: Recent Foraminifera. *W. Junk*, The Haugue, 1–515.

Bown P.R. 1998: Calcareous Nannofossil Biostratigraphy. British Micropalaeontological Society, Publications Series, *Chapman & Hall*, London, 1–315.

Chernyshev I.V., Konečný V., Lexa J., Kovalenker V.A., Jeleň S., Lebedev V.A & Goltsman Y.V. 2013: K–Ar and Rb–Sr geochronology and evolution of the Štiavnica Stratovolcano (Central Slovakia). *Geol. Carpath.* 64, 327–351. https://doi.org/10.2478/geoca-2013-0023

Cicha I., Rögl F., Rupp Ch. & Čtyroká J. (Eds.) 1998: Oligocene–Miocene foraminifera of the Central Paratethys. *Abhandlungen der Senckenbergischen Naturforschenden Gesellschaft* 549, 1–325.

Coe A.L. (Ed.) 2003: The sedimentary record of sea-level change. *Cambridge University Press*, Cambridge, 1–288.

Collinson J.D. & Thompson D.B. 1989: Sedimentary structures. 2nd ed. *Chapman and Hall*, London, 1–207.

Ellis B., Daly D.C., Hickey L.J., Johnson K., Mitchell J.D., Wilf P. & Wing S. 2009: Manual of Leaf Architecture. *Cornell University Press*, Cambridge, 1–190.

Filipescu S., Miclea A., Gross M., Harzhauser M., Zágoršek K. & Jipa C. 2014: Early Sarmatian paleoenvironments in the easternmost Pannonian Basin (Borod Depression, Romania) revealed by the micropaleontological data. *Geol. Carpath.* 65, 67–81. https://doi.org/10.2478/geoca-2014-0005

Fordinál K. & Elečko M. 2000: Ripňany Formation–a Sarmatian and Early Pannonian fresh water sedimentary assemblage of the Rišňovce depression. *Mineralia Slovaca* 32, 55–60.

Fusán O., Biely A., Ibrmajer J., Plančár J. & Rozložník L. 1987: Basement of the Tertiary of the inner West Carpathians. *Geological Institute of Dionýz Štúr*, Bratislava, 1–123 (in Slovak).

Harzhauser M. 2002: Marine und brachyhaline Gastropoden aus dem Karpatium des Korneuburger Beckens und der Kreuzstettener Bucht (Österreich, Untermiozän). *Beiträge zur Paläontologie* 27, 61–159.

Harzhauser M. & Piller W.E. 2004: Integrated stratigraphy of the Sarmatian (Upper Middle Miocene) in the western Central Paratethys. *Stratigraphy* 1, 65–86.

Harzhauser M. & Piller E.W. 2007: Benchmark data of a changing sea – Palaeogeography, Palaeobiogeography and events in the Central Paratethys during the Miocene. *Palaeogeogr. Palaeoclimatol. Palaeoecol.* 253, 8–31. https://doi.org/10.1016/j.palaeo.2007.03.031

Harzhauser M., Grunert P., Mandic O., Lukeneder P., García Gallardo Á., Neubauer T.A., Carnevale G., Landau B.M., Sauer R. & Strauss P. 2018: Middle and Late Badenian palaeoenvironments in the northern Vienna Basin and their potential link to the Badenian Salinity Crisis. *Geol. Carpath.* 69, 129–168. https://doi.org/10.1515/geoca-2018-0009

Hohenegger J., Ćorić S. & Wagreich M. 2014: Timing of the Middle Miocene Badenian Stage of the Central Paratethys. *Geol. Carpath.* 65, 55–66. https://doi.org/10.2478/geoca-2014-0004

Hók J., Šujan M. & Šipka F. 2014: Tectonic division of the Western Carpathians: An overview and a new approach. *Acta Geologica Slovaca* 6, 135–143 (in Slovak with English abstract).

Hók J., Kováč M., Pelech O., Pešková I., Vojtko R. & Králiková S. 2016: The Alpine tectonic evolution of the Danube Basin and its northern periphery (southwestern Slovakia). *Geol. Carpath.* 67, 495–505. https://doi.org/10.1515/geoca-2016-0031

Holcová K. 2008: Foraminiferal species diversity in the Central Paratethys – a reflection of global or local events? *Geol. Carpath.* 59, 71–85.

Holcová K., Dašková J., Fordinál K., Hrabovský J., Milovský R., Scheiner F. &Vacek F. 2019: A series of ecostratigraphic events across the Langhian/Serravallian boundary in an epicontinental setting: the northern Pannonian Basin. *Facies* 65, 1–22. https://doi.org/10.1007/s10347-019-0576-1

Holbourn A., Kuhnt W., Clemens S., Prell W. & Andersen N. 2013: Middle to late Miocene stepwise climate cooling: Evidence from a high-resolution deep water isotope curve spanning 8 million years. *Paleoceanography* 28, 688–699. https://doi.org/10.1002/2013PA002538

Horváth F., Musitz B., Balázs A., Végh A., Uhrin A., Nádor A., Koroknai B., Pap N., Tóth T. & Wórum G. 2015: Evolution of the Pannonian Basin and its geothermal resources. *Geothermics* 53, 328–352. https://doi.org/10.1016/j.geothermics.2014.07.009

Hyžný M., Hudáčková N., Biskupič R., Rybár S., Fuksi T., Halásová E., Zágoršek K., Jamrich M. & Ledvák P. 2012: Devínska Kobyla – a window into the Middle Miocene shallow-water marine environments of the Central Paratethys (Vienna Basin, Slovakia). *Acta Geologica Slovaca* 4, 5–21.

Káčer Š., Antalík M., Lexa J., Zvara I., Fritzman R., Vlachovič J., Bystrická G., Brodnianska M., Potfaj M., Madarás J., Nagy A., Maglay J., Ivanička J., Gross P., Rakús M., Vozárová A., Buček S., Boorová D., Šimon L., Mello J., Polák M., Bezák V., Hók J., Teťák F., Konečný V., Kučera M., Žec B., Elečko M., Hraško Ľ., Kováčik M. & Prostaš J. 2005: Digital geological map of Slovakia, 1:50,000. Map server. *Stage geological institute of Dionýz Štúr*, Bratislava.

Konečný V. (Ed.), Lexa J., Halouzka R., Hók J., Vozár J., Dublan L., Nagy A., Šimon L., Havrila M., Ivanička J., Hojstovičová V., Mihálíková A., Vozárová A., Konečný P., Kováčikova M., Filo M., Marcin D., Klukanová A., Liščák P. & Žáková E. 1998: Explanations to the geological map of Štiavnica Mts. and Pohronský Inovec Mts. (Štiavnica stratovolcano). *State geological insitute of Dionýz Štur*, Bratislava, 1–473 (in Slovak with English summary).

Kováč M. 2000: Geodynamic, palaeogeographical and structural evolution of the Carpathian–Pannonian region during the Miocene. *VEDA*, Bratislava, 1–202 (in Slovak).

Kováč M., Rybár S., Halásová E., Hudáčková N., Šarinová K., Šujan M., Baranyi V., Kováčová M., Ruman A., Klučiar T. & Zlinská A. 2018: Changes in Cenozoic depositional environment and sediment provenance in the Danube Basin. *Basin Research* 30, 97–131. https://doi.org/10.1111/bre.12244

Kováčová P. & Hudáčková N. 2009: Late Badenian foraminifers from the Vienna basin (Central Paratethys): Stable isotope study and paleoecological implications. *Geol. Carpath.* 60, 59–70. https://doi.org/10.2478/v10096-009-0006-3

Loeblich A.R. & Tappan H. 1992: Present status of Foraminiferal Classification. In: Takayanagi Y. & Saito T. (Eds.): Studies in Benthic Foraminifera: Proceedings of the Fourth symposium on benthic foraminifera. *Tokai University Press*, Sendai, 93–102.

Lowe D.R. & LoPiccolo R.D. 1974: The characteristics and origins of dish and pillar structures. *J. Sediment. Petrol.* 44, 484–501.

Mandic O. 2004: Pectinid bivalves from the Grund Formation (Lower Badenian, Middle Miocene, Alpine-Carpathian Foredeep) – taxonomic revision and stratigraphic significance. *Geol. Carpath.* 55, 129–146.

Mandic O., Sant K., Kallanxhi M-E., Ćorić S., Theobalt D., Grunert P., de Leeuw A. & Krijgsman W. 2018: Integrated bio-magnetostratigraphy of the Badenian reference section Ugljevik in southern Pannonian Basin – implications for the Paratethys history (middle Miocene, Central Europe). *Global Planet. Change* 172, 374–395. https://doi.org/10.1016/j.gloplacha.2018.10.010

Martini E. 1971: Standard Tertiary and Quaternary Calcareous Nannoplankton Zonation. In: Farinacci A. (Ed.): Proceedings of the II Planktonic Conference, Roma, 1970. *Edizioni Tecnoscienza*, 739–785.

Miall A.D. 2006: The geology of fluvial deposits. *Springer*, New York, 1–582.

Mikuž V. 2009: Miocene gastropods from the vicinity of Šentjernej and from other localities in the Krka Basin, Slovenia. *Folia Biologica et Geologica* 50, 5–69.

Murray J.W. 2006: Ecology and Applications of Benthic Foraminifera. *Cambridge University Press*, Cambridge, 1–426.

Nagy A., Halouzka R., Konečný V., Lexa J., Fordinál K., Havrila M., Vozár J., Liščák P., Stolár M., Benková K. & Kubeš P. 1998: Explanatory notes to geological map of Danube Lowlands, eastern part 1:50,000. *Geological Survey of Slovak Republic*, Bratislava, 1–187 (in Slovak).

Nemec W. 1990: Aspects of sediment movement on steep delta slopes. In: Colella A. & Prior D.B. (Eds): Coarse-grained Deltas. *Blackwell Scientific Publications*, Oxford, 29–73.

Németh K. & Martin U. 2007: Practical volcanology: lecture notes for understanding volcanic rocks from field based studies. *Occasional Papers of the Geological Institute of Hungary* 207, 1–221. ISBN 978-963-671-259-4

Neuwerth R., Suter F., Guzman C.A. & Gorin G.E. 2006: Soft-sediment deformation in a tectonically active area: The Plio-Pleistocene Zarzal Formation in the Cauca Valley (Western Colombia). *Sediment. Geol.* 186, 67–88. https://doi.org/10.1016/j.sedgeo.2005.10.009

Nichols G. 2009: Sedimentology and Stratigraphy (2nd Edition). *Wiley-Blackwell*, Hoboken, New Jersey, 1–419.

Oszczypko-Clowes M., Lelek D. & Oszczypko N. 2012: Sarmatian paleoecological environment of the Machów Formation based on the quantitative nannofossil analysis – a case study from the Sokołów area (Polish Carpathian Foredeep). *Geol. Carpath.* 63, 267–294. https://doi.org/10.2478/v10096-012-0022-6

Papp A. 1954: Die Molluskenfauna im Sarmat des Wiener Beckens. *Mitteilungen der Geologischen Gesellschaft in Wien* 45, 1–112.

Patruno S. & Helland-Hansen W. 2018: Clinoforms and clinoform systems: Reviw and dynamic classification scheme for shorelines, subaqueous deltas, shelf edges and continental margins. *Earth-Sci. Rev.* 185, 202–233. https://doi.org/10.1016/j.earscirev.2018.05.016

Paulissen W.E., Luthi S.M.1, Grunert P., Ćorić S. & Harzhauser M. 2011: Integrated high-resolution stratigraphy of a Middle to Late Miocene sedimentary sequence in the central part of the Vienna Basin *Geol. Carpath.* 62, 155–169. https://doi.org/10.2478/v10096-011-0013-z

Pavelić D. 2001: Tectonostratigraphic model for the North Croatian and North Bosnian sector of the Miocene Pannonian Basin System. *Basin Research* 13, 359–376. https://doi.org/10.1046/j.0950-091x.2001.00155.x

Pavelić D. 2005: Cyclicity in the evolution of the Neogene North Croatian basin (Pannonian Basin System). In: Mabesoone J.M. & Neumann V.H. (Eds.): Cyclic Development of Sedimentary Basins. *Dev. Sedim. Elsevier* 57, 273–283.

Pavelić D. & Kovačić M. 2018: Sedimentology and stratigraphy of the Neogene rift-type North Croatian Basin (Pannonian Basin System, Croatia): A review. *Mar. Petrol. Geol.* 91, 455–469. https://doi.org/10.1016/j.marpetgeo.2018.01.026

Peryt D., Gedl P. & Peryt T.M. 2014: Foraminiferal and palynological records of the Late Badenian (Middle Miocene) transgression in Podolia (Shchyrets near Lviv, western Ukraine). *Geol. Quarterly* 58, 445–464.

Piller W.E & Harzhauser M. 2005: The myth of the brackish Sarmatian Sea. *Terra Nova* 17, 450–455. https://doi.org/10.1111/j.1365-3121.2005.00632.x

Piller W., Harzhauser M. & Mandic O. 2007: Miocene Central Paratethys stratigraphy – current status and future directions. *Stratigraphy* 4, 151–168.

Radivojević D., Rundić L. & Knežević S. 2010: Geology of the Čoka structure in northern Banat (Central Paratethys, Serbia). *Geol. Carpath.* 61, 341–352. https://doi.org/10.2478/v10096-010-0020-5

Rossi V.M., Perillo M.M., Steel R.J. & Olariu C. 2017: Quantifying mixed-process variability in shallow-marine depositional systems: What are sedimentary structures really telling us? *J. Sediment. Res.* 87, 1060–1074. https://doi.org/10.2110/jsr.2017.49

Ruman A., Rybár S., Hudáčková N., Šujan M. & Halásová E. 2017: Depositional environment changes during the early–late Serravallian boundary dated by the Central Paratethys bioevents. *Facies* 63, 1–13. https://doi.org/10.1007/s10347-016-0490-8

Rybár S., Kováč M., Šarinová K., Halásová E., Hudáčková N., Šujan M., Kováčová M., Ruman A. & Klučiar T. 2016: Neogene changes in paleogeography, paleoenvironment and the provenance of sediment in the northern Danube Basin. *Bull. Geosci.* 91, 367–398. https://doi.org/10.3140/bull.geosci.1571

Rybár S., Šarinová K., Sant K., Kuiper K.F., Kováčová M.,Vojtko R., Reiser M.K., Fordinál K., Teodoridis V., Nováková P. & Vlček T. 2019: New $^{40}Ar/^{39}Ar$, fission track and sedimentological data on a middle Miocene tuff occurring in the Vienna Basin: Implications for the north-western Central Paratethys region. *Geol. Carpath.* 70, 386–404. https://doi.org/10.2478/geoca-2019-0022

Sant K., Palcu D.V., Mandic O. & Krijgsman W. 2017: Changing seas in the Early-Middle Miocene of central Europa: a Mediterranean approach to Paratethyan stratigraphy. T*erra Nova* 29, 5, 273–281. https://doi.org/10.1111/ter.12273

Sant K., Kuiper F.K., Rybár S., Grunert P., Harzhauser M., Mandic O., Jamrich M., Šarinová K., Hudáčková N. & Krijgsman W. 2020: $^{40}Ar/^{39}Ar$ geochronology using high sensitivity mass spectrometry: Examples from middle Miocene horizons of the Central Paratethys. *Geol. Carpath.* 71, 166–182. https://doi.org/10.31577/GeolCarp.71.2.5

Schultz O. 2001: Bivalvia neogenica (Nuculacea-Unionacea). In: Piller W.E. (Ed.): Catalogus Fossilium Austriae. *Verlag der Österreichischen Akademie der Wissenschaften* 1, 1–380.

Schultz O. 2003: Bivalvia neogenica (Lucinoidea-Mactroidea).In: Piller W.E. (Ed.): Catalogus Fossilium Austriae. *Verlag der Österreichischen Akademie der Wissenschaften* 1, 381–690.

Schultz O. 2005: Bivalvia neogenica (Solenoidea-Clavagelloidea). In: Piller W.E. (Ed.): Catalogus Fossilium Austriae. *Verlag der Österreichischen Akademie der Wissenschaften* 1, 691–1212.

Seneš J., Franko O., Koštálik J. & Porubský A. 1962: Explanatory notes to geological map 1: 200,000, Nové Zámky–Čalovo. *Geofond*, Bratislava, 1–151 (in Slovak).

Senešová M. 1980: Analyses of mollusks necrocenosis (synchronous tanatocenosis), an example from early Badenian of south Slovakia. Doctoral thesis. *Archive of the Department of Geology and Paleontology, Comenius University in Bratislava*, 1–45 (in Slovak).

Strausz L. 1966: Die Miozän-Mediterranen Gastropoden Ungarns. *Akadémiai Kiadó*, Budapest, 1–693.

Sztanó O., Kováč M., Magyar I., Šujan M., Fodor L., Uhrin A., Rybár S., Csillag G. & Tőkés L. 2016: Late Miocene sedimentary record of the Danube/Kisalföld Basin: interregional correlation of depositional systems, stratigraphy and structural evolution. *Geol. Carpath.* 67, 525–542. https://doi.org/10.1515/geoca-2016-0033

Śliwiński M., Bąbel M., Nejbert K., Olszewska-Nejbert D., Gąsiewicz A., Schreiber B.Ch., Benowitz J.A. & Layer P. 2012: Badenian–Sarmatian chronostratigraphy in the Polish Carpathian Foredeep. *Palaeogeogr. Palaeoclimatol. Palaeoecol.* 326–328, 12–19. https://doi.org/10.1016/j.palaeo.2011.12.018

Šarinová K., Rybár S., Halásová E., Hudáčková N., Jamrich M., Kováčová M. & Šujan M. 2018: Integrated biostratigraphical, sedimentological and provenance analyses with implications for lithostratigraphic ranking: the Miocene Komjatice depression of the Danube Basin. *Geol. Carpath.* 69, 382–409. https://doi.org/10.1515/geoca-2018-0023

Šujan M., Braucher R., Kováč M., Bourlès D.L., Rybár S., Guillou V. & Hudáčková N. 2016: Application of the authigenic $^{10}Be/^{9}Be$ dating method to Late Miocene–Pliocene sequences in the Northern Danube Basin (Pannonian Basin System): Confirmation of heterochronous evolution of sedimentary environments. *Global Planet. Change* 137, 35–53. https://doi.org/10.1016/j.gloplacha.2015.12.013

Švagrovsky J. 1971: Das Sarmat der Tschechoslowakei und seine Molluskenfauna. *Acta Geologica et Geographica universitatis comenianae Geologica* 20, 1–473.

Tari G., Báldi T. & Báldi-Béke M. 1993: Paleogene retroarc flexural basin beneath the Neogene Pannonian Basin: a geodynamic model. *Tectonophysics* 226, 433–456.

Teodoridis V., Kovar-Eder J. & Mazouch P. 2011: The IPR-vegetation analysis applied to modern vegetation in SE China and Japan. *PALAIOS* 26, 10, 623–638. https://doi.org/10.2110/palo.2010.p10-149r

Vaškovský I., Bárta R., Hanzel V., Halouzka R., Harčáč J., Karolus K., Pristaš J., Remšík A., Šucha P., Vass D. & Vaškovská E. 1982: Explanatory notes to geological map of Danube Lowlands, southeastern part 1:50,000. *State geological insitute of Dionýz Štur*, Bratislava, 1–115 (in Slovak with English summary).

Vass D. 2002: Lithostratigraphy of Western Carpathians: Neogene and Buda Paleogene. *State Geological Institute of Dionýz Štúr*, 1–200 (in Slovak).

Wang C-W. 1961: The Forests of China with a Survey of Grassland and Desert Vegetation. Publication Series No. 5. *Maria Moors Cabot Foundation*. *Harvard University*, Cambridge, 1–313.

Young J.R. 1998: Neogene. In: Bown P.R. (Ed.): Calcareous Nannofossil Biostratigraphy. *British Micropalaeontological Society, Publications Series*. *Chapman & Hall*, London, 225–265.

Young J.R., Bown P.R. & Lees J.A. 2017: Nannotax3 website. International Nannoplankton Association. Accessed 21 Apr. 2017. http://www.mikrotax.org/Nannotax3

Appendix

Table 1: Coordinates of the studied sections.

Section	M.a.s.l.	X	Y
Kamenica nad Hronom 1	125	47°49’50.81”N	18°42’41.10”E
Kamenica nad Hronom 2	160	47°50’34.14”N	18°43’54.66”E
Lontov	129	48°02’03.49”N	18°46’56.24”E
Kubáňovo	129	48°03’26.44”N	18°48’22.14”E
Zbrojníky	177	48°06’34.87”N	18°43’03.37”E
Hontianska Vrbica	180	48°08’44.12”N	18°42’23.51”E
Kamenec	207	48°15’20.75”N	18°39’57.86”E
Podlužany	190	48°14’39.61”N	18°36’45.55”E
Tlmače	180	48°17’26.42”N	18°31’16.38”E

Supplement

Table S1: Fossil content recorded in studied samples.

Sections	Sample	Discipline	Zone/Subzone	Assemblages
Kamenica nad Hronom 2	**KH2-1** (10/Sm)	F	Late Badenian	*Ammonia inflata, A. Viennensis, Amphistegina* sp., *Biasterigerina planorbis, Cibicidoides pachyderma, Elphidium crispum, E. Macellum, Heterolepa dutemplei, Miliolidae* indet., *Cycloforina badenensis*
		N	Late Badenian	*Coccolithus pelagicus, Discoaster cf. exilis, Reticulofenestra minuta, R. haqii, Braarudosphaera bigelowii parvula*
		Other	Unassigned	Mollusk shells, biotite, non-rounded quartz, sponge spicules, diatoms
Kamenica nad Hronom 2	**KH2-2** (60/Sm)	F	Late Badenian	*Ammonia* sp., *Biasterigerina planorbis, Hanzawaia boueana, Glandulina ovula, Heterolepa dutemplei*
		N	Unassigned	Barren
		Other	Unassigned	Diatoms, Mollusk shells: *Ancilla glandiformis*, *Cerithium procrenatum*, *Cerithium vulgatum*, *Linga columbella* and *Turritella* sp.
Kamenica nad Hronom 1	**KH1-2** (KHD/Lt)	F	Unassigned	*Ammonia inflata, Miliolidae* indet.
		N	Unassigned	Barren
		Other	Unassigned	Barren
Kamenica nad Hronom 1	**KH1-1** (KHD2/Tb)	F	Unassigned	Barren
		N	Unassigned	Barren
		Other	Unassigned	Sponge spicules
Kamenica nad Hronom 1	**KH1-3** (Ct/Lt)	F	Unassigned	Barren
		N	Unassigned	Barren
		Other	Unassigned	Echinoide spines, bryozoans Plant assemblages: *Daphnogene polymorpha, Laurophyllum* sp. 1 (slender and oblong leaves), *Laurophylum* sp. 2 (broadly ovate to obovate leaves) and *Ternstroemites* sp.
Lontov	**LON-1** (Fl)	F	Unassigned	*Bolivina antiqua, Bolivina dilatata, Ciperoella ciperoensis, Globorotalia transsylvanica*
		N	Late Badenian/ Sarmatian	*Braarudosphaera bigelowii parvula*, *Calcidiscus leptoporus, C. pataecus*, *Coccolithus formosus*, *C. miopelagicus*, *C. pelagicus*, *Cribrosphaerella ehrenbergii, Cyclicargolithus floridanus*, *Discoaster barbadiensis, D. deflandrei, D.* sp., *Helicosphaera ampliaperta, H. carteri, H. euphratis, H. scissura, H.* sp., *H. walbersdorfensis, H. wallichii, Holodiscolithus macroporus, Micula staurophora, Pontosphaera alta, P. multipora, Reticulofenestra bisecta, R. excavate, R. haqii, R. minuta, R. pseudoumbilicus, R. umbilicus, Rhabdosphaera sicca, Sphenolithus heteromorphus, S. moriformis, Syracosphaera sp., Thoracosphaera, Tribrachiatus orthostylus, Triquetrorhabdulus carinatus, Umbilicosphaera Jafari*, U. *rotula*, *Zeugrhabdotus embergeri, Zygrhablithus bijugatus*
		Other	Unassigned	Diatoms, radiolarians, sponge spicules, mollusk shells
Lontov	**LON-2** (SW/Gp)	F	Early Sarmatian	*Ammonia parkinsoniana, Ammonia viennensis, Elphidium josephinum, E. Macellum, E. Reginum, Miliolidae* indet., *Porosononion martkobi, Schackoinella imperatoria*
		N	Late Badenian/ Sarmatian	The same as sample 1
		Other	Unassigned	Ostracods Mollusk shells: *Cerithium procrenatum*, *Cerithium rubiginosum*, *Granulolabium bicinctum*, *Duplicata duplicate*, *Euspira helicina sarmatica* and *Vitta picta*
Tlmače	**TL-2** (Fm)	F	Unassigned	Barren
		N	Unassigned	Barren
		Other	Sarmatian	Mollusk shells: *Mohrensternia* sp., *Rissoa* sp., *Abra* sp., *Inaeqnicostata politioanei suessiforme*, *Limnocardium* sp., *Loripes* sp. and *Loripes* aff. *dujardini*
Hontianska Vrbica	**HON-2** (Fl)	F	Unassigned	Barren
		N	Unassigned	Barren
		Other	Sarmatian	Sponge spicules, fossil leaves Mollusk shells: *Cerastoderma* cf. *latisulcum*, *Cerastoderma latisulcum nexingense* and *Cardiidae* indet.

Table S1 (continued): Fossil content recorded in studied samples.

Sections	Sample	Discipline	Zone/Subzone	Assemblages
Kubáňovo	**KUB-1** (Fm)	F	?Sarmatian	*Ammonia inflata, Protoglobobulimina pupoides, Cancris auricula, Elphidium* sp., *Globigerina concinna, Globigerinoides* sp.
		N	Unassigned	Barren
		Other	Unassigned	Diatoms, sponge spicules, fossil leaves
Kamenec	**KAM-1** (F)	F	Unassigned	?*Ammobaculites* sp.?
		N	Unassigned	Barren
		Other	Unassigned	Rare bivalvia shells
Zbrojníky	**ZBR-2** (Sla)	F	Unassigned	Barren
		N	Unassigned	Barren
		Other	Unassigned	Sponge spicules
Zbrojníky	**ZBR-1** (Gt)	F	Unassigned	Barren
		N	Unassigned	Barren
		Other	Unassigned	Large mammals
Podlužany	**POD-1** (Gt)	F	Unassigned	*Fursenkoina* sp.
		N	Unassigned	Barren
		Other	Unassigned	Sponge spicules, large mammals
Podlužany	**POD-2** (St)	F	Unassigned	Barren
		N	Unassigned	Barren
		Other	Unassigned	Barren

Table S2: Chemical composition of amphibole, pyroxene and plagioclase.

Amphibole

Kamenica nad Hronom 1: amphibole (calculated after Hawthorn et al. 2018)									
	dated tuff								
	phenoc. volc. lith. 1	clast 1	phenoc. core volc. lith. 2	phenoc. rim volc. lith. 2	clast 2 core	clast 3 core	clast 4	clast 5	clast 6
Species	**mag.-hastingsite**	**ferri-sadanagaite**	**ferri-sadanagaite**	**sadanagaite**	**tschermakite**	**mag.-ferri-hornblende**	**magnesio-hornblende**	**magnesio-ferri-hornblende**	**ferri-tschermakite**
SiO_2	41.09	41.69	44.65	43.77	42.39	42.80	42.58	43.64	43.74
TiO_2	1.86	1.42	1.09	1.22	1.23	1.32	1.17	1.14	1.16
Al_2O_3	15.66	14.04	11.08	11.78	12.69	11.90	12.77	11.49	11.79
Cr_2O_3	0.00	0.03	0.02	0.00	0.03	0.00	0.00	0.00	0.05
MnO	0.27	0.35	0.40	0.45	0.32	0.43	0.32	0.36	0.40
FeO	15.05	19.25	19.73	20.17	19.67	20.65	18.90	19.84	20.25
NiO	0.00	0.00	0.00	0.00	0.04	0.00	0.00	0.00	0.01
MgO	11.01	8.56	9.61	9.49	8.99	9.16	9.03	9.10	9.25
CaO	9.87	10.37	9.86	9.48	10.47	9.60	10.73	9.96	9.82
Na_2O	2.31	1.56	1.44	1.49	1.56	1.51	1.38	1.36	1.46
K_2O	0.64	0.76	0.43	0.42	0.64	0.51	0.62	0.49	0.48
F	0.00	0.00	0.00	0.00	0.00	0.00	0.00	0.00	0.00
Cl	0.08	0.14	0.10	0.10	0.13	0.13	0.13	0.12	0.11
O=F,Cl (calc)	−0.02	−0.03	−0.02	−0.02	−0.03	−0.03	−0.03	−0.03	−0.02
Initial Total	*97.81*	*98.15*	*98.41*	*98.35*	*98.11*	*97.98*	*97.59*	*97.49*	*98.51*
Si	6.247	5.859	5.961	6.037	6.202	6.584	6.497	6.306	6.367
AlT	1.753	2.141	2.039	1.963	1.798	1.416	1.503	1.694	1.633
T subtotal	*8.000*	*8.000*	*8.000*	*8.000*	*8.000*	*8.000*	*8.000*	*8.000*	*8.000*
Ti	0.247	0.214	0.246	0.206	0.159	0.121	0.136	0.138	0.147
AlC	0.215	0.323	0.266	0.748	0.664	0.510	0.557	0.531	0.453
Cr	0.006	0.006	0.000	0.000	0.004	0.003	0.000	0.003	0.000
Fe^{3+}	0.567	0.835	0.798	0.425	0.587	0.595	0.441	0.664	0.783
Ni	0.000	0.002	0.000	0.000	0.000	0.000	0.000	0.005	0.000
$Mn^{2+}C$	0.000	0.000	0.000	0.000	0.000	0.000	0.000	0.000	0.000
$Fe^{2+}C$	1.747	0.337	0.913	1.211	1.689	1.659	1.766	1.667	1.585
Mg	2.217	3.282	2.777	2.411	1.897	2.112	2.100	1.993	2.031
C subtotal	*4.999*	*4.999*	*5.000*	*5.001*	*5.000*	*5.000*	*5.000*	*5.001*	*4.999*
$Mn^{2+}B$	0.035	0.021	0.025	0.033	0.045	0.050	0.056	0.040	0.055
$Fe^{2+}B$	0.082	0.069	0.073	0.214	0.119	0.179	0.297	0.116	0.201
Ca	1.750	1.809	1.789	1.553	1.653	1.558	1.508	1.668	1.530
NaB	0.133	0.102	0.112	0.200	0.184	0.214	0.139	0.176	0.215
B subtotal	*2.000*	*2.001*	*1.999*	*2.000*	*2.001*	*2.001*	*2.000*	*2.000*	*2.001*
NaA	0.415	0.521	0.471	0.458	0.266	0.199	0.291	0.275	0.221
K	0.188	0.130	0.125	0.121	0.143	0.081	0.080	0.122	0.096
A subtotal	*0.603*	*0.651*	*0.596*	*0.579*	*0.409*	*0.280*	*0.371*	*0.397*	*0.317*
O (non-W)	22.000	22.000	22.000	22.000	22.000	22.000	22.000	22.000	22.000
OH	1.928	1.993	1.988	1.981	1.964	1.974	1.974	1.967	1.968
Cl	0.072	0.007	0.012	0.019	0.036	0.026	0.026	0.033	0.032
W subtotal	*2.000*	*2.000*	*2.000*	*2.000*	*2.000*	*2.000*	*2.000*	*2.000*	*2.000*
Sum T,C,B,A	15.602	15.651	15.595	15.580	15.410	15.281	15.371	15.398	15.317

Table S2 (continued): Chemical composition of amphibole, pyroxene and plagioclase.

Amphibole

Kamenica nad Hronom 1: amphibole (calculated after Hawthorn et al. 2018)											
	lower lapilli tuff										
	phenoc. volc. lith. 1	phenoc. volc. lith. 1	phenoc. volc. lith. 1	phenoc. light zone volc. lith.2	phenoc. dark zone volc. lith.2	phenoc. volc. lith.3	phenoc. volc. lith.3	phenoc. volc. lith.3	phenoc. volc. lith.3	clast 1	clast 2
Species	**magnesio-hastingsite**	**magnesio-hastingsite**	**magnesio-hastingsite**	**magnesio-hastingsite**	**magnesio-hastingsite**	**pargasite**	**magnesio-hastingsite**	**magnesio-hastingsite**	**magnesio-hastingsite**	**magnesio-ferri-hornblende**	**magnesio-ferri-hornblende**
SiO_2	43.93	40.97	42.77	42.91	42.78	43.33	42.01	41.48	43.22	44.87	42.88
TiO_2	2.11	1.96	2.47	1.28	1.03	2.63	1.61	1.72	1.63	1.48	1.79
Al_2O_3	11.10	14.10	11.32	13.73	14.73	11.28	15.11	14.73	13.21	10.45	12.81
Cr_2O_3	0.01	0.00	0.03	0.01	0.01	0.00	0.03	0.00	0.03	0.00	0.00
MnO	0.33	0.19	0.31	0.23	0.11	0.29	0.10	0.15	0.17	0.40	0.28
FeO	15.12	12.05	15.75	12.67	7.18	16.03	8.96	9.77	9.69	16.55	14.34
NiO	0.01	0.00	0.02	0.00	0.01	0.00	0.00	0.00	0.00	0.01	0.00
MgO	12.65	13.18	11.98	13.53	16.81	11.65	15.37	15.03	15.56	12.02	12.79
CaO	11.03	11.52	10.85	11.19	12.07	10.95	11.89	12.08	11.86	10.32	10.96
Na_2O	2.02	2.12	1.87	1.97	2.28	1.92	2.23	2.22	2.19	1.58	1.89
K_2O	0.56	0.75	0.66	0.59	0.48	0.71	0.61	0.60	0.56	0.54	0.62
F	0.00	0.00	0.00	0.00	0.00	0.00	0.00	0.00	0.00	0.00	0.00
Cl	0.09	0.05	0.12	0.07	0.02	0.16	0.03	0.02	0.04	0.13	0.05
O=F,Cl (calc)	−0.02	−0.01	−0.03	−0.02	0.00	−0.04	−0.01	−0.01	−0.01	−0.03	−0.01
Initial Total	*98.95*	*96.90*	*98.11*	*98.17*	*97.52*	*98.89*	*97.94*	*97.81*	*98.16*	*98.32*	*98.40*
Si	6.381	6.027	6.292	6.188	6.065	6.365	6.004	5.966	6.182	6.543	6.218
AlT	1.619	1.973	1.708	1.812	1.935	1.635	1.996	2.034	1.818	1.457	1.782
T subtotal	*8.000*	*8.000*	*8.000*	*8.000*	*8.000*	*8.000*	*8.000*	*8.000*	*8.000*	*8.000*	*8.000*
Ti	0.231	0.217	0.273	0.139	0.109	0.291	0.174	0.186	0.176	0.162	0.195
AlC	0.282	0.472	0.254	0.522	0.526	0.317	0.548	0.463	0.409	0.339	0.408
Cr	0.001	0.000	0.004	0.001	0.001	0.000	0.003	0.000	0.003	0.000	0.000
Fe^{3+}	0.502	0.517	0.554	0.638	0.694	0.284	0.560	0.616	0.539	0.657	0.654
Ni	0.001	0.000	0.002	0.000	0.001	0.000	0.000	0.000	0.000	0.001	0.000
$Mn^{2+}C$	0.000	0.000	0.000	0.000	0.000	0.000	0.000	0.000	0.000	0.000	0.000
$Fe^{2+}C$	1.244	0.904	1.286	0.791	0.115	1.557	0.440	0.513	0.556	1.228	0.979
Mg	2.740	2.890	2.627	2.909	3.553	2.551	3.275	3.222	3.317	2.613	2.763
C subtotal	*5.001*	*5.000*	*5.000*	*5.000*	*4.999*	*5.000*	*5.000*	*5.000*	*5.000*	*5.000*	*4.999*
$Mn^{2+}B$	0.041	0.024	0.039	0.028	0.013	0.035	0.012	0.019	0.021	0.050	0.034
$Fe^{2+}B$	0.092	0.062	0.097	0.099	0.043	0.128	0.072	0.046	0.064	0.133	0.105
Ca	1.717	1.815	1.710	1.729	1.834	1.723	1.821	1.862	1.818	1.612	1.702
NaB	0.150	0.098	0.154	0.144	0.110	0.114	0.095	0.074	0.097	0.205	0.158
B subtotal	*2.000*	*1.999*	*2.000*	*2.000*	*2.000*	*2.000*	*2.000*	*2.001*	*2.000*	*2.000*	*1.999*
NaA	0.418	0.508	0.379	0.408	0.518	0.434	0.521	0.547	0.510	0.243	0.374
K	0.104	0.140	0.125	0.109	0.087	0.132	0.112	0.110	0.103	0.100	0.114
A subtotal	*0.522*	*0.648*	*0.504*	*0.517*	*0.605*	*0.566*	*0.633*	*0.657*	*0.613*	*0.343*	*0.488*
O (non-W)	22.000	22.000	22.000	22.000	22.000	22.000	22.000	22.000	22.000	22.000	22.000
OH	1.979	1.987	1.969	1.984	1.996	1.961	1.994	1.994	1.991	1.968	1.989
Cl	0.021	0.013	0.031	0.016	0.004	0.039	0.006	0.006	0.009	0.032	0.011
W subtotal	*2.000*	*2.000*	*2.000*	*2.000*	*2.000*	*2.000*	*2.000*	*2.000*	*2.000*	*2.000*	*2.000*
Sum T,C,B,A	15.523	15.647	15.504	15.517	15.604	15.566	15.633	15.658	15.613	15.343	15.486

Table S2 (continued): Chemical composition of amphibole, pyroxene and plagioclase.

Amphibole

Tlmače: heavy fraction from conglomerate													
	heavy fraction from conglomerate (grain-size fraction 0.25–0.10 mm)												
	clast 1 rim	clast 2	clast 3	clast 4	clast 5	clast 6	clast 7	clast 8 core	clast 8 rim	clast 9	clast 10	clast 11	clast 12
Species	magnesio-ferri-hornblende	Ti-rich magnesio-hastingsite	magnesio-hastingsite	Ti-rich magnesio-hastingsite	magnesio-hastingsite	magnesio-ferri-hornblende	Ti-rich magnesio-hastingsite	magnesio-ferri-hornblende	pargasite	magnesio-hastingsite	pargasite	magnesio-hastingsite	Ti-rich magnesio-hastingsite
SiO_2	43.55	41.89	44.19	41.77	43.84	43.97	39.86	46.24	44.48	43.56	44.58	44.29	41.70
TiO_2	1.87	2.66	1.60	2.90	1.52	1.90	3.12	1.28	2.31	1.83	2.14	1.99	2.82
Al_2O_3	7.88	9.66	7.72	11.56	7.66	8.61	10.96	6.77	8.51	8.65	8.74	8.98	11.82
Cr_2O_3	0.05	0.00	0.00	0.01	0.02	0.01	0.02	0.00	0.00	0.00	0.00	0.00	0.01
MnO	0.51	0.43	0.56	0.20	0.58	0.32	0.52	0.63	0.39	0.58	0.26	0.58	0.21
FeO	18.11	17.48	19.53	13.37	19.45	17.35	17.58	18.91	16.88	18.34	16.43	17.36	12.03
NiO	0.04	0.00	0.00	0.00	0.00	0.00	0.00	0.00	0.00	0.00	0.01	0.02	0.00
MgO	11.03	10.58	9.68	12.87	9.85	11.32	9.53	10.49	11.04	10.51	11.41	10.85	13.60
CaO	10.51	10.81	10.90	11.18	11.05	10.90	11.34	11.17	10.97	10.36	11.08	10.54	11.30
Na_2O	1.78	1.98	1.47	2.10	1.52	1.57	2.06	1.36	1.68	1.73	1.55	1.81	2.07
K_2O	0.63	0.83	0.93	0.72	0.92	0.85	0.74	0.65	0.76	0.60	0.89	0.59	0.76
F	0.00	0.00	0.00	0.00	0.00	0.00	0.00	0.00	0.00	0.00	0.00	0.00	0.00
Cl	0.11	0.13	0.32	0.02	0.27	0.25	0.16	0.12	0.13	0.12	0.21	0.11	0.05
O=F,Cl (calc)	−0.02	−0.03	−0.07	−0.01	−0.06	−0.06	−0.04	−0.03	−0.03	−0.03	−0.05	−0.02	−0.01
Initial Total	*96.04*	*96.43*	*96.83*	*96.70*	*96.61*	*96.98*	*95.84*	*97.60*	*97.13*	*96.23*	*97.26*	*97.08*	*96.36*
Si	6.626	6.401	6.769	6.210	6.713	6.612	6.161	6.961	6.691	6.637	6.684	6.658	6.186
AlT	1.374	1.599	1.231	1.790	1.287	1.388	1.839	1.039	1.309	1.363	1.316	1.342	1.814
T subtotal	*8.000*	*8.000*	*8.000*	*8.000*	*8.000*	*8.000*	*8.000*	*8.000*	*8.000*	*8.000*	*8.000*	*8.000*	*8.000*
Ti	0.214	0.306	0.185	0.324	0.175	0.215	0.363	0.145	0.261	0.209	0.241	0.225	0.315
AlC	0.038	0.142	0.163	0.236	0.095	0.139	0.158	0.162	0.200	0.190	0.229	0.249	0.251
Cr	0.006	0.000	0.000	0.001	0.003	0.001	0.003	0.000	0.000	0.000	0.000	0.000	0.001
Fe^{3+}	0.558	0.261	0.234	0.397	0.408	0.457	0.320	0.215	0.193	0.348	0.199	0.283	0.409
Ni	0.004	0.000	0.000	0.000	0.000	0.000	0.000	0.000	0.000	0.000	0.002	0.002	0.000
$Mn^{2+}C$	0.000	0.000	0.000	0.000	0.000	0.000	0.011	0.000	0.000	0.000	0.000	0.000	0.000
$Fe^{2+}C$	1.678	1.881	2.207	1.188	2.071	1.651	1.952	2.125	1.870	1.865	1.781	1.810	1.015
Mg	2.502	2.410	2.211	2.853	2.249	2.537	2.195	2.354	2.476	2.387	2.550	2.431	3.008
C subtotal	*5.000*	*5.000*	*5.000*	*4.999*	*5.001*	*5.000*	*5.002*	*5.001*	*5.000*	*4.999*	*5.002*	*5.000*	*4.999*
$Mn^{2+}B$	0.066	0.055	0.072	0.025	0.075	0.040	0.057	0.081	0.049	0.075	0.032	0.073	0.027
$Fe^{2+}B$	0.068	0.093	0.062	0.077	0.013	0.074	0.000	0.042	0.061	0.124	0.081	0.090	0.069
Ca	1.713	1.769	1.789	1.782	1.813	1.757	1.878	1.802	1.769	1.692	1.780	1.697	1.797
NaB	0.152	0.083	0.076	0.116	0.100	0.129	0.065	0.075	0.121	0.110	0.106	0.140	0.108
B subtotal	*1.999*	*2.000*	*1.999*	*2.000*	*2.001*	*2.000*	*2.000*	*2.000*	*2.000*	*2.001*	*1.999*	*2.000*	*2.001*
NaA	0.374	0.505	0.360	0.488	0.352	0.329	0.552	0.324	0.368	0.400	0.345	0.388	0.486
K	0.123	0.162	0.181	0.136	0.179	0.162	0.146	0.124	0.146	0.116	0.169	0.112	0.145
A subtotal	*0.497*	*0.667*	*0.541*	*0.624*	*0.531*	*0.491*	*0.698*	*0.448*	*0.514*	*0.516*	*0.514*	*0.500*	*0.631*
O (non-W)	22.000	22.000	22.000	22.000	22.000	22.000	22.000	22.000	22.000	22.000	22.000	22.000	22.000
OH	1.972	1.967	1.918	1.994	1.929	1.937	1.959	1.968	1.966	1.970	1.946	1.973	1.989
Cl	0.028	0.033	0.082	0.006	0.071	0.063	0.041	0.032	0.034	0.030	0.054	0.027	0.011
W subtotal	*2.000*	*2.000*	*2.000*	*2.000*	*2.000*	*2.000*	*2.000*	*2.000*	*2.000*	*2.000*	*2.000*	*2.000*	*2.000*
Sum T,C,B,A	15.496	15.667	15.540	15.623	15.533	15.491	15.700	15.449	15.514	15.516	15.515	15.500	15.631

Table S2 (continued): Chemical composition of amphibole, pyroxene and plagioclase.

Pyroxene

Kamenica nad Hronom 1						Tlmače				
	lower lapilli tuff			lower lapilli tuff		heavy fraction from conglomerate (grain-size fraction 0.25–0.10 mm)				
	orthopyroxene			clinopyroxene						
	phenocryst volc. lith.3	clast		phenocryst volc. lith.1	clast	clasts 1	clasts 2	clasts 3 core	clasts 3 rim	clasts 4
species	enstatite	enstatite	species	pigeonite	pigeonite	diopside	diopside	augite	diopside	diopside
SiO_2	52.30	53.12	SiO_2	50.03	50.55	46.78	51.72	50.06	49.12	52.92
TiO_2	0.26	0.24	TiO_2	0.19	0.23	1.53	0.16	0.40	0.62	0.26
Al_2O_3	2.21	1.96	Al_2O_3	1.71	1.77	7.10	1.34	1.57	3.67	1.70
Cr_2O_3	0.00	0.00	Cr_2O_3	0.03	0.00	0.59	1.08	0.12	0.98	0.62
FeO	22.05	19.98	FeO	19.50	19.04	2.87	0.07	9.28	1.22	2.66
MgO	22.07	23.63	Fe_2O_3	4.54	3.70	3.94	3.20	2.02	3.73	1.14
MnO	0.83	0.67	MgO	19.59	20.16	13.74	17.87	13.34	16.05	17.30
CaO	1.20	1.43	MnO	0.84	0.87	0.09	0.09	0.30	0.14	0.07
Na_2O	0.00	0.00	CaO	3.67	3.55	22.14	22.89	20.03	21.78	22.68
K_2O	0.00	0.00	Na_2O	0.01	0.06	0.33	0.14	0.26	0.31	0.19
Total	*100.92*	*101.03*	K_2O	0.01	0.00	0.00	0.00	0.00	0.00	0.00
Si	1.934	1.942	*Total*	*100.11*	*99.93*	*99.11*	*98.55*	*97.38*	*97.62*	*99.55*
Al	0.066	0.058	Si	1.892	1.904	1.748	1.911	1.931	1.845	1.938
sum T	*2.000*	*2.000*	Al	0.076	0.079	0.252	0.058	0.069	0.155	0.062
Al	0.031	0.026	Fe^{3+}	0.032	0.018	0.000	0.031	0.000	0.000	0.000
Ti	0.007	0.007	*sum T*	*2.000*	*2.000*	*2.000*	*2.000*	*2.000*	*2.000*	*2.000*
Cr	0.000	0.000	Al	0.000	0.000	0.061	0.000	0.003	0.008	0.012
Mg	1.217	1.288	Fe^{3+}	0.097	0.087	0.111	0.058	0.059	0.105	0.031
Fe^{2+}	0.682	0.611	Ti	0.005	0.007	0.043	0.004	0.012	0.018	0.007
Mn	0.026	0.021	Cr	0.001	0.000	0.017	0.032	0.004	0.029	0.018
Ca	0.048	0.056	Mg	0.896	0.906	0.765	0.906	0.767	0.840	0.932
sum	*2.010*	*2.009*	Fe^{2+}	0.000	0.000	0.003	0.000	0.157	0.000	0.000
			sum M1	*1.000*	*1.000*	*1.000*	*1.000*	*1.000*	*1.000*	*1.000*
			Mg^{2+}	0.208	0.225	0.000	0.079	0.000	0.059	0.013
			Fe^{2+}	0.617	0.600	0.087	0.002	0.143	0.038	0.082
			Mn	0.027	0.028	0.003	0.003	0.010	0.004	0.002
			Ca	0.149	0.143	0.887	0.907	0.828	0.877	0.890
			Na	0.000	0.004	0.024	0.010	0.019	0.023	0.013
			sum M2	*1.001*	*1.000*	*1.001*	*1.000*	*1.000*	*1.001*	*1.000*

Table S2 (continued): Chemical composition of amphibole, pyroxene and plagioclase.

Pyroxene

Tlmače											
	heavy fraction from conglomerate (grain-size fraction 0.25–0.10 mm)										
	clasts 5	clasts 6	clasts 7	clasts 8	clasts 9	clasts 10	clasts 11 core	clasts 11 rim	clasts 12	clasts 13	clasts 14
species	diopside	diopside	diopside	augite	diopside	diopside	augite	diopside	diopside	diopside	diopside
SiO_2	48.71	50.54	51.59	51.25	45.22	51.64	51.98	51.09	53.01	52.38	52.93
TiO_2	0.90	0.25	0.42	0.43	1.99	0.71	0.35	0.84	0.28	0.42	0.21
Al_2O_3	4.52	1.94	1.99	2.75	7.51	3.72	1.58	4.00	2.16	2.93	1.37
Cr_2O_3	0.35	0.64	0.12	0.78	0.42	0.20	0.06	0.79	0.85	0.83	0.46
FeO	1.77	0.37	3.04	3.79	2.34	4.13	11.02	4.71	3.14	2.99	2.79
Fe_2O_3	3.85	3.99	2.74	1.72	4.92	1.35	0.00	0.44	0.44	0.93	1.29
MgO	15.03	16.99	16.46	16.75	13.05	15.88	13.02	15.27	16.91	16.23	17.30
MnO	0.10	0.12	0.14	0.21	0.14	0.17	0.32	0.13	0.08	0.10	0.14
CaO	22.62	22.55	22.28	20.65	22.44	21.99	20.25	22.40	22.72	23.10	22.54
Na_2O	0.31	0.22	0.22	0.29	0.31	0.35	0.28	0.23	0.25	0.29	0.18
K_2O	0.00	0.00	0.01	0.00	0.00	0.00	0.01	0.00	0.00	0.01	0.00
Total	*98.16*	*97.61*	*98.99*	*98.63*	*98.34*	*100.14*	*98.87*	*99.90*	*99.84*	*100.21*	*99.22*
Si	1.826	1.892	1.913	1.903	1.710	1.891	1.971	1.881	1.936	1.912	1.946
Al	0.174	0.086	0.087	0.097	0.290	0.109	0.029	0.119	0.064	0.088	0.054
Fe^{3+}	0.000	0.022	0.000	0.000	0.000	0.000	0.000	0.000	0.000	0.000	0.000
sum T	*2.000*	*2.000*	*2.000*	*2.000*	*2.000*	*2.000*	*2.000*	*2.000*	*2.000*	*2.000*	*2.000*
Al	0.026	0.000	0.000	0.023	0.045	0.051	0.042	0.054	0.029	0.038	0.006
Fe^{3+}	0.109	0.090	0.076	0.048	0.140	0.037	0.000	0.012	0.012	0.025	0.036
Ti	0.026	0.007	0.012	0.012	0.056	0.020	0.010	0.023	0.008	0.012	0.006
Cr	0.010	0.019	0.003	0.023	0.013	0.006	0.002	0.023	0.025	0.024	0.014
Mg	0.830	0.884	0.909	0.894	0.736	0.867	0.736	0.838	0.921	0.883	0.939
Fe^{2+}	0.000	0.000	0.000	0.000	0.010	0.019	0.210	0.050	0.006	0.018	0.000
sum M1	*1.000*	*1.000*	*1.000*	*1.000*	*1.000*	*1.000*	*1.000*	*1.000*	*1.000*	*1.000*	*1.000*
Mg^{2+}	0.010	0.065	0.001	0.033	0.000	0.000	0.000	0.000	0.000	0.000	0.009
Fe^{2+}	0.055	0.012	0.094	0.118	0.064	0.107	0.140	0.096	0.091	0.073	0.086
Mn	0.003	0.004	0.004	0.007	0.004	0.005	0.010	0.004	0.003	0.003	0.004
Ca	0.909	0.905	0.885	0.821	0.909	0.863	0.823	0.884	0.889	0.903	0.888
Na	0.023	0.016	0.015	0.021	0.023	0.025	0.020	0.017	0.018	0.021	0.013
sum M2	*1.000*	*1.001*	*1.001*	*1.000*	*1.001*	*1.000*	*0.993*	*1.000*	*1.000*	*1.001*	*1.000*

Table S2 (continued): Chemical composition of amphibole, pyroxene and plagioclase.

Plagioclase

Kamenica nad Hronom 1													
	dated tuff												
	phenoc. core volc. lith.1	phenoc. rim volc. lith.1	phenoc. core volc. lith.2	phenoc. rim volc. lith.2	phenoc. core volc. lith.3	phenoc. rim volc. lith.3	phenoc.1 rim volc. lith.4	phenoc.1 core volc. lith.4	phenoc.2 volc. lith.4	phenoc. volc. lith.5	phenoc. volc. lith.6	clast1 core	clast1 rim
SiO_2	50.94	53.71	43.83	51.05	48.12	56.41	51.42	55.29	54.50	55.11	56.46	47.47	54.76
Al_2O_3	30.92	28.53	32.49	26.92	33.73	29.16	30.12	28.19	28.28	29.49	28.29	33.30	28.06
SrO	0.13	0.13	0.11	0.12	0.11	0.11	0.12	0.12	0.10	0.09	0.13	0.11	0.11
FeO	0.11	0.13	0.14	0.10	0.10	0.11	0.10	0.10	0.09	0.09	0.15	0.09	0.10
MgO	0.00	0.00	0.00	0.00	0.00	0.00	0.00	0.00	0.00	0.00	0.01	0.00	0.00
CaO	13.96	11.80	17.33	11.53	17.06	11.41	13.47	11.12	11.19	12.06	10.97	17.26	10.76
Na_2O	3.77	4.89	1.57	4.80	1.91	5.18	3.83	5.19	5.14	4.96	5.43	1.94	5.52
K_2O	0.12	0.21	0.04	0.23	0.06	0.22	0.14	0.22	0.22	0.19	0.22	0.06	0.24
Total	*99.95*	*99.42*	*95.51*	*94.74*	*101.09*	*102.59*	*99.20*	*100.23*	*99.53*	*101.99*	*101.67*	*100.23*	*99.54*
Si	2.324	2.447	2.120	2.446	2.185	2.481	2.358	2.490	2.474	2.445	2.505	2.178	2.485
Al	1.662	1.532	1.852	1.520	1.805	1.511	1.628	1.496	1.513	1.542	1.479	1.801	1.501
Sr	0.003	0.003	0.003	0.003	0.003	0.003	0.003	0.003	0.003	0.002	0.003	0.003	0.003
Fe	0.004	0.005	0.006	0.004	0.004	0.004	0.004	0.004	0.004	0.003	0.005	0.004	0.004
Mg	0.000	0.000	0.000	0.000	0.000	0.000	0.000	0.000	0.000	0.000	0.001	0.000	0.000
Ca	0.682	0.576	0.898	0.592	0.830	0.538	0.662	0.536	0.544	0.573	0.522	0.848	0.523
Na	0.333	0.432	0.147	0.445	0.168	0.442	0.341	0.453	0.453	0.427	0.467	0.172	0.486
K	0.007	0.012	0.003	0.014	0.003	0.012	0.008	0.012	0.013	0.011	0.012	0.003	0.014
cat sum	*5.016*	*5.009*	*5.029*	*5.024*	*4.998*	*4.991*	*5.003*	*4.995*	*5.002*	*5.003*	*4.995*	*5.009*	*5.015*
orthoclase	0.71	1.20	0.24	1.31	0.35	1.25	0.78	1.23	1.27	1.05	1.24	0.32	1.33
albite	32.58	42.35	14.03	42.39	16.77	44.55	33.72	45.23	44.84	42.24	46.67	16.82	47.51
anortite	66.71	56.45	85.72	56.30	82.88	54.20	65.50	53.54	53.89	56.71	52.08	82.86	51.16

Kamenica nad Hronom 1															
	lower lapilli tuf														
	phenoc.1 volc. lith.1	phenoc.2 volc. lith.1	phenoc.3 volc. lith.1	phenoc. volc. lith.2	microlith1 volc. lith.2	microlith2 volc. lith.2	phenoc.1 volc. lith.3	phenoc.2 volc. lith.3	phenoc.3 volc. lith.3	microlith volc. lith.3	microlith rim volc. lith.4	phenoc. rim volc. lith.4	clast 1	clast 2	clast 3
SiO_2	46.97	49.05	48.80	46.49	51.80	47.28	47.06	48.43	47.51	48.80	57.74	54.09	46.07	48.77	45.79
Al_2O_3	33.23	32.81	31.14	33.66	28.51	33.46	32.81	32.46	33.29	31.26	25.96	28.73	32.02	33.16	34.20
SrO	0.07	0.08		0.10	0.08	0.05	0.09	0.11	0.10	0.09	0.10	0.08	0.08	0.08	0.07
FeO	0.33	0.37	0.31	0.54	0.85	0.46	0.36	0.33	0.35	0.53	0.24	0.11	0.38	0.35	0.31
MgO	0.01	0.00	0.03	0.04	0.18	0.02	0.02	0.03	0.01	0.09	0.01	0.00	0.01	0.01	0.01
CaO	17.46	16.37	16.08	17.83	12.75	17.62	17.02	16.39	16.78	15.37	8.68	12.06	16.92	16.80	18.27
Na_2O	1.72	2.43	2.57	1.52	3.89	1.67	1.81	2.36	1.95	2.66	6.28	4.75	2.17	2.01	1.19
K_2O	0.06	0.08	0.11	0.05	0.18	0.04	0.08	0.08	0.06	0.11	0.34	0.16	0.11	0.08	0.04
Total	*99.85*	*101.19*	*99.12*	*100.22*	*98.24*	*100.59*	*99.25*	*100.18*	*100.05*	*98.91*	*99.36*	*99.98*	*97.75*	*101.26*	*99.90*
Si	2.167	2.224	2.256	2.142	2.401	2.165	2.182	2.220	2.183	2.262	2.606	2.448	2.175	2.210	2.116
Al	1.807	1.753	1.697	1.827	1.558	1.806	1.793	1.754	1.802	1.708	1.381	1.533	1.782	1.771	1.863
Sr	0.002	0.002	0.000	0.003	0.002	0.001	0.003	0.003	0.003	0.003	0.003	0.002	0.002	0.002	0.002
Fe	0.013	0.014	0.012	0.021	0.033	0.018	0.014	0.013	0.013	0.020	0.009	0.004	0.015	0.013	0.012
Mg	0.001	0.000	0.002	0.003	0.013	0.001	0.001	0.002	0.001	0.006	0.001	0.000	0.000	0.001	0.001
Ca	0.863	0.795	0.797	0.880	0.633	0.865	0.846	0.805	0.826	0.763	0.420	0.585	0.856	0.816	0.904
Na	0.154	0.214	0.231	0.136	0.350	0.148	0.162	0.210	0.173	0.239	0.550	0.416	0.199	0.177	0.107
K	0.003	0.005	0.006	0.003	0.011	0.003	0.005	0.005	0.003	0.006	0.019	0.009	0.006	0.005	0.003
cat sum	*5.008*	*5.008*	*5.000*	*5.014*	*5.000*	*5.007*	*5.005*	*5.010*	*5.004*	*5.007*	*4.988*	*4.998*	*5.036*	*4.995*	*5.008*
orthoclase	0.32	0.46	0.62	0.29	1.09	0.25	0.45	0.44	0.34	0.64	1.96	0.90	0.60	0.47	0.26
albite	15.07	21.07	22.31	13.36	35.21	14.58	16.03	20.57	17.29	23.70	55.58	41.21	18.72	17.72	10.55
anortite	84.62	78.47	77.08	86.36	63.70	85.17	83.52	78.98	82.37	75.66	42.46	57.89	80.68	81.81	89.19